Available online at www.sciencedirect.com

ScienceDirect

Geochimica et Cosmochimica Acta xxx (2020) xxx–xxx

Geochimica et Cosmochimica Acta

www.elsevier.com/locate/gca

Basinal hydrographic and redox controls on selenium enrichment and isotopic composition in Paleozoic black shales

Michael A. Kipp [a,b,*], Thomas J. Algeo [c,d,e], Eva E. Stüeken [b,f], Roger Buick [a,b]

[a] Department of Earth & Space Sciences and Astrobiology Program, University of Washington, Seattle, WA 98195-1310, USA
[b] Virtual Planetary Laboratory, NASA Nexus for Exoplanet System Science, Seattle, WA 98195-1310, USA
[c] Department of Geology, University of Cincinnati, Cincinnati, OH 45221-0013, USA
[d] State Key Laboratory of Biogeology and Environmental Geology, China University of Geosciences, Wuhan 430074, China
[e] State Key Laboratory of Geological Processes and Mineral Resources, China University of Geosciences, Wuhan 430074, China
[f] School of Earth & Environmental Sciences, University of St. Andrews, St. Andrews, Fife, KY16 9AL Scotland, United Kingdom

Received 14 July 2019; accepted in revised form 13 December 2019; available online xxxx

Abstract

Mass-dependent variations in selenium stable isotope ratios have recently been developed as a paleo-redox proxy. Since the reduction of selenium oxyanions occurs at a relatively high redox potential, this system holds promise for probing conditions relevant to the evolution and diversification of eukaryotic and animal life, which required substantial dissolved oxygen levels. Although several studies have identified selenium isotopic variability during oxygenation events in Earth's distant past, we still have only a broad understanding of the mechanisms controlling this isotopic variability. This currently limits the robust interpretation of selenium isotope variability to first-order mechanisms driving large-magnitude changes. Here, we explore selenium isotope variability within and among Paleozoic black shales deposited on the North American craton that have been well-studied using a variety of other paleo-environmental proxies. Using this combined dataset, we attempt to unravel the controls on selenium abundance and isotope ratios in organic-rich ancient marine sedimentary rocks. We find that in the Late Pennsylvanian units, an estuarine nutrient trap on the Midcontinent Shelf enabled vigorous selenium recycling, leading to very high concentrations in sediments and enrichment of heavy isotopes in the aqueous selenium reservoir. In contrast, we find that among the Late Devonian units, differences in local basinal hydrography led to a gradient in selenium abundance and isotopic fractionation, with the more restricted basins depleting their selenium reservoirs and causing enrichment of heavy isotopes in the residual aqueous reservoir. In both of these case studies, the additional context provided by complementary paleo-environmental proxies was critical for distinguishing between possible drivers of selenium isotopic variability. When extending such studies to other paleo-environmental settings, we suggest that the continued use of complementary datasets will enable the most robust use of the selenium paleo-redox proxy. Moreover, further development of techniques for high-precision and phase-specific selenium isotope measurements will greatly improve the ability to deduce subtle redox fluctuations with this proxy.

Keywords: Selenium isotopes; Epicontinental seas, late Paleozoic; Basin hydrography; Redox proxies; Redox-sensitive trace elements

1. INTRODUCTION

Evaluating the redox state of ancient seawater is a key aspect of studying Earth's environmental evolution. This task is critical to the study of rising oxygen levels through-

* Corresponding author at: Division of Geological & Planetary Sciences, California Institute of Technology, Pasadena, CA 91125, USA.
E-mail address: mkipp@caltech.edu (M.A. Kipp).

https://doi.org/10.1016/j.gca.2019.12.016
0016-7037/

out geologic history (*e.g.*, Lyons et al., 2014), environmental triggers of early animal evolution (*e.g.*, Sperling et al., 2013), kill mechanisms of mass extinction events (*e.g.*, Wignall and Twitchett, 1996), and even oceanographic mechanisms of carbon storage on glacial-interglacial timescales (*e.g.*, Anderson et al., 2019). As such, the paleoceanographic toolkit is always being refined to include novel paleo-redox proxies with ever-more precise informative power.

Over the last two decades there has been a surge of interest in trace element proxies for paleo-redox conditions (Tribovillard et al., 2006; Anbar and Gordon, 2008; Algeo et al., 2012; Little et al., 2015). Studies of redox-sensitive trace metal enrichment have proven greatly informative of first-order secular trends in Earth's stepwise oxygenation (Scott et al., 2008; Partin et al., 2013) and transient anoxic events in the more recent past (Brumsack, 2006). Taking this a step further, the field of "non-traditional" stable isotope geochemistry has recently grown into a discipline of its own (e.g., Teng et al., 2017), creating a potentially richer source of information about oxidation-reduction reactions in a variety of paleo-environmental settings.

Some redox-sensitive trace element isotopic systems have already yielded a wealth of information about modern and ancient redox processes in seawater. For instance, molybdenum (Mo) isotopes in sulfidic black shales have become a well-established proxy for the global extent of sulfidic seawater (*e.g.*, Siebert et al., 2003; Gordon et al., 2009; Kendall et al., 2017) and have allowed inferences about the secular oxygenation of the Earth's ocean over billion-year timescales (*e.g.*, Arnold et al., 2004; Dahl et al., 2010; Kendall et al., 2011; Chen et al., 2015; Kendall et al., 2015). Uranium (U) isotopes in carbonates have recently joined Mo as a quantitatively powerful global-ocean redox proxy, with sensitivity to the areal extent of anoxic sediments (cf. Tissot and Dauphas, 2015), and they have been used to study a wide range of events in deep time (Lau et al., 2016; Lau et al., 2017; Clarkson et al., 2018; Zhang et al., 2018; Tostevin et al., 2019). An advantage of both the Mo and U proxies is that these elements have long residence times of $> 10^5$ yr in the modern ocean and therefore have the potential to capture global redox conditions.

In addition to inferences about redox conditions in the global ocean, more localized redox assessments have been enabled by proxies such as the iodine content of carbonates (Lu et al., 2010, 2018). As iodate (IO_3^-) is quickly reduced to iodide (I^-) in suboxic water (*e.g.*, Rue et al., 1997), iodate incorporation in carbonates is only possible under fairly well-oxygenated waters (Lu et al., 2010). This high redox potential of the iodine system allows interrogation of redox fluctuations close to thresholds that are relevant to eukaryotic – including animal – life. However, without multiple stable isotopes the iodine system is less amenable to quantitative flux reconstructions than its aforementioned counterparts.

Although the above proxies all have demonstrable power in evaluating redox conditions in ancient seawater, there are gaps in their spatial, temporal and redox sensitivities that might be filled by other trace element systems. The selenium (Se) system is promising in this respect, since the high redox potential of Se oxyanion reduction is similar to that of iodate and nitrate (*e.g.*, Rue et al., 1997; Fig. 1). Furthermore, the marine residence time of Se (10^3–10^4 yr) is of a similar order of magnitude to the ocean mixing time (Broecker and Peng, 1982), and possibly much shorter under anoxic conditions, meaning that it is likely not globally homogenized and thus yields more localized redox information than the Mo and U systems. Selenium isotopes should therefore respond to global and regional perturbations on relatively short timescales. With six stable isotopes and an ability to shift between the −II, 0, +IV and +VI oxidation states in seawater (Cutter and Bruland, 1984), the Se system has the potential to encode a wealth of information about redox reactions in the marine environment. Despite this potential, Se isotopes remain much less studied than the aforementioned proxies.

There are several factors that conspire to make Se a difficult system to investigate. Selenium volatilization during wet chemical sample preparation can alter Se concentrations and isotopic compositions (Chau and Riley 1965; Kurzawa et al., 2017), requiring vigilance during digestion and evaporation. Furthermore, Se is typically introduced to the MC-ICP-MS via a hydride generator (HG-MC-ICP-MS) in order to improve signal strength, but this apparatus can be a source of signal instability (Rouxel et al., 2002). Even following successful introduction to the plasma, Se measurements are complicated by isobaric interferences from germanium, arsenic, krypton and – most insidiously – argon (Ar), which confounds analysis of the most abundant Se isotope (^{80}Se) through interference with Ar dimers (reviewed in Stüeken et al., 2013). Beyond these analytical challenges, Se is generally present at low abun-

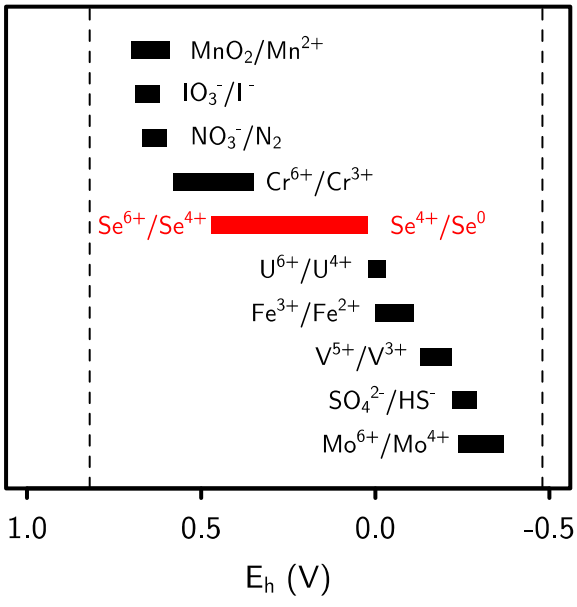

Fig. 1. **Redox potentials of redox couplets commonly utilized in paleo-redox studies.** Data generated for a pH range of 7–8. Dashed lines denote stability field of liquid water. Reduction of selenium oxyanions begins at relatively high redox potentials, similar to the range for iodate and nitrate reduction (Rue et al., 1997).

Please cite this article in press as: Kipp M. A., et al. Basinal hydrographic and redox controls on selenium enrichment and isotopic composition in Paleozoic black shales. *Geochim. Cosmochim. Acta* (2020), https://doi.org/10.1016/j.gca.2019.12.016

dances in geological materials (ng/g to μg/g; Rouxel et al., 2002; Mitchell et al., 2012; Stueken et al., 2015a,b,c; Kurzawa et al., 2017), often requiring the digestion of large amounts of sample to obtain sufficient Se for analysis. Despite these complications, however, recent methodological developments in both the chemical preparation and analytical environment of Se isotope analysis have successively pushed this system toward the realm of routine analysis (*e.g.*, Stüeken et al., 2013; Pogge von Strandmann et al., 2014; Kurzawa et al., 2017), opening up the possibility that Se isotopes can soon enter the standard toolkit of paleoceanographers.

Although these techniques have enabled the study of Se isotopic variability in a wide range of settings (*e.g.*, soils, Schilling et al., 2011; groundwater, Basu et al., 2016; lakes, Clark and Johnson, 2010; laboratory, Johnson and Bullen, 2003; Ellis et al., 2003), large gaps remain in our understanding of the behavior of Se and its isotopes across redox gradients in the modern ocean and during (de-)oxygenation events in Earth's past. Here, we leverage a wealth of data from other redox-sensitive elements to better evaluate the similarities and differences between the Se system and other proxies. Specifically, we focus on two sample sets of well-characterized black shales deposited on the North American continent during the late Paleozoic Era in two intervals: (a) the Late Pennsylvanian and (b) the Late Devonian. We measured Se concentrations and isotopic ratios in 65 samples from these units and compared the data to a variety of paleo-environmental indicators. In particular, we sought to determine the effects of watermass restriction and local redox conditions on Se abundance and isotopic fractionation in these two settings. In doing so, we aimed to elucidate the mechanisms responsible for the observed variability in Se isotope ratios and enrichment factors among the study units, with broader implications for the further development of Se as a paleoceanographic proxy.

2. SELENIUM GEOCHEMISTRY

2.1. The selenium cycle

Selenium is a trace constituent of the upper continental crust, with a mean concentration of ~60 ng/g (Stüeken, 2017). Crustal Se is predominantly found in sulfide minerals, with Se substituting for sulfur. The Se isotopic composition (here and throughout the text reported in delta notation as $\delta^{82/78}$Se relative to Se NIST SRM 3149; Carignan and Wen, 2007) of the upper continental crust is estimated to be $\sim 0.0 \pm 0.5$‰ (Stüeken, 2017) based on analyses of representative igneous reservoirs (Rouxel et al., 2002; Kurzawa et al., 2017; Yierpan et al., 2018). The range of $\delta^{82/78}$Se values observed in bulk marine sediments deposited across all of Earth's history is approximately −3‰ to +3‰ (Stüeken et al., 2015b; Mitchell et al., 2016), indicating that isotopic fractionation of Se occurs during biogeochemical cycling.

The dominant input of Se to the modern ocean is oxidative continental weathering, whereby Se^{-II} in crustal sulfides is oxidized to Se^{IV} or Se^{VI}, which form highly soluble oxyanions. The process of oxidative weathering typically induces rather small isotopic fractionations (<0.5‰; Johnson et al., 1999; Schilling et al., 2011). Weathering of exceptionally Se-rich shales (up ~2 wt. % Se) has been shown to enable larger fractionations (Zhu et al., 2014), though this wide range is neither thought to be representative of most weathering environments nor of net global inputs, because in that particular case secondary Se cycling was facilitated by unusually large amounts of organic matter in the rocks. Given generally small fractionations during weathering and transport, the riverine supply of Se to the ocean is thought to have an isotopic composition similar to the upper continental crust (~0‰). Additional Se input from volcanic gases (which can contain H_2Se) plays a minor role in the global Se budget today (Mosher and Duce, 1987; Floor and Román-Ross 2012; Stüeken, 2017), but could conceivably have been more important early in Earth's history prior to the onset of significant oxidative continental weathering in the late Archean (Stüeken et al., 2012). The isotopic composition of volcanic Se has not been directly constrained, but it is thought that this flux does not substantially alter the marine Se isotope mass balance (Stüeken, 2017).

Upon reaching the ocean, Se is scavenged in the photic zone as an essential micronutrient, yielding nutrient-type profiles in the ocean (Measures et al., 1980; Measures and Burton, 1980). The biological pump is the dominant vector of Se transport from surface waters to the deep ocean and marine sediments. Selenium has a short residence time (~2–3 yr) as Se oxyanions in surface waters (Cutter and Bruland, 1984) and an intermediate residence time (10^3–10^4 yr, similar to oceanic mixing times) as regenerated Se oxyanions in the deep ocean (Broecker and Peng, 1982; Cutter and Bruland, 1984). The bioassimilation of Se by phytoplankton generally imparts a small isotopic fractionation (<0.5‰; Clark and Johnson, 2010), which may be negligible when uptake is quantitative. The isotopic composition of Se in planktonic biomass is thus thought to approximate that of dissolved Se in seawater (Stüeken et al., 2015b; Stüeken, 2017).

Owing to its low concentration (~1–2 nM), there are few direct measurements of Se isotope ratios in seawater. A recently developed method for determining the concentration and isotopic composition of Se in seawater yielded $\delta^{82/78}$Se values (scaled from $\delta^{82/76}$Se assuming mass-dependent fractionation) of +0.27‰ for deep waters of the NW Pacific Ocean (Chang et al., 2017). This closely agrees (within a 1σ analytical precision of ±0.1–0.2‰; cf. Mitchell et al., 2012; Stüeken et al., 2015b, 2015c; this study) with a single measurement of phytoplankton biomass (+0.27‰; Mitchell et al., 2012), a single measurement of a deep-sea Fe-Mn nodule (+0.32‰; Rouxel et al., 2004), and mass balance calculations estimating the Se-isotopic composition of seawater as ~+0.3‰ (Stüeken, 2017).

Marine sediments are commonly enriched in Se. Sediments deposited in oxic, open-ocean settings over the last ~500 kyr have an average (geometric mean) Se concentration of 0.68 μg/g (95% confidence interval of 0.55–0.83, $n = 100$), whereas sediments deposited in anoxic settings have systematically higher Se concentrations (geom. mean = 2.18 μg/g; 95% confidence interval of 1.46–

Please cite this article in press as: Kipp M. A., et al. Basinal hydrographic and redox controls on selenium enrichment and isotopic composition in Paleozoic black shales. *Geochim. Cosmochim. Acta* (2020), https://doi.org/10.1016/j.gca.2019.12.016

3.27 μg/g, $n = 38$) (data compiled in Stüeken et al., 2015b). For this reason, the study of Se isotopes as a paleo-redox proxy has thus far focused predominantly on reducing marine sediments, which typically have moderate to high Se concentrations. Our understanding of the processes controlling Se enrichment and isotopic fractionation in these settings is reviewed below.

2.2. The selenium isotope paleo-redox proxy

The removal of Se to marine sediments and fractionation of Se isotopes are driven by multiple biogeochemical processes. Remineralization of organic matter in sediments results in the release of some bioassimilated Se, the fate of which is redox dependent. In oxic facies, adsorption of the Se^{IV} ion selenite onto Fe-Mn-oxides can be significant (cf. Balistrieri and Chao, 1990; Rovira et al., 2008). In reducing facies (*i.e.*, the targets of the present study), seawater Se removal follows two main pathways: (a) the burial of biologically-assimilated Se in organic matter, and (b) the sequestration of Se through dissimilatory reduction of oxyanions to inorganic Se^0 or Se^{-II} phases. The relative importance of these two burial pathways is poorly constrained, though limited phase-specific Se measurements in modern settings suggest that the resulting Se pools (*i.e.*, organic-bound Se derived from export production and Se^0 or sulfide-hosted Se^{-II} derived from dissimilatory oxyanion reduction) can comprise roughly similar proportions of total sedimentary Se (Velinsky and Cutter, 1990).

The first route is likely dominated by organic matter exported from the photic zone, where primary productivity is highest and phytoplankton have a nutritional demand for Se. The second route chiefly involves reductive immobilization of Se oxyanions liberated from biomass in deep waters or sediment porewaters. At reduction potentials similar to that of nitrate reduction (Fig. 1), Se oxyanions are reduced first to Se^0 and then potentially further to Se^{-II} (Oremland et al., 1989). Fully reduced Se^{-II} can substitute for sulfur in diagenetic sulfide minerals (*e.g.*, pyrite), which provide a stable host phase for Se on geological timescales due to the stoichiometric incorporation of Se in the mineral structure (Large et al., 2014, and references therein). Processes surrounding the burial of Se^0 are less well constrained. Reduction to Se^0 generates nanoparticles that can sink out of the water column and accumulate in sediments (Oremland et al., 1989; Velinsky and Cutter, 1990). It is unclear to what extent these particles withstand diagenetic and metamorphic conditions, but some amount of Se^0 appears to be recoverable from ancient marine sedimentary rocks (Kulp and Pratt, 2004; Wen et al., 2007). It is likely, though, that subsequent reduction to Se^{-II} on diagenetic timescales enables a considerable degree of Se incorporation into sulfides, as the Se content of pyrite in ancient marine sedimentary rocks (Kulp and Pratt, 2004; Fan et al., 2011) far exceeds the amounts detected in modern sediments (Velinsky and Cutter, 1990).

The bulk Se isotopic composition of reduced marine sediments is a function of both the biogenic (*i.e.*, organic-bound) fraction and the reductively immobilized (*i.e.*, elemental and sulfide-bound) fraction. Due to the generally small isotopic fractionations associated with biological uptake and remineralization (Johnson and Bullen 2004; Clark and Johnson, 2010), the Se isotopic composition of biomass in marine sediments is thought to fairly closely match that of dissolved Se in the surface ocean (~+0.3‰; Mitchell et al., 2012; Stüeken et al., 2015b). In contrast, Se sequestered through oxyanion reduction can become substantially isotopically lighter than seawater if the process is non-quantitative, as Se reduction exerts a large kinetic isotopic preference for lighter isotopes (as much as −12‰; Johnson and Bullen, 2004). Non-quantitative reduction is thought to be prevalent in sediments with suboxic porewaters or bottom waters that are connected to a large, oxic reservoir of Se oxyanions, thereby allowing renewed Se supply and precluding complete consumption of the dissolved Se pool.

Modern environments that likely harbor non-quantitative Se reduction include open-marine settings such as the mid-Atlantic (Johnson and Bullen, 2004), the Bermuda Rise (Shore, 2011), and the Arabian Sea (Mitchell et al., 2012). Bulk marine sediments from these open-marine settings over the last ~500 kyr are slightly isotopically depleted relative to seawater ($\delta^{82/78}Se = -0.10 \pm 0.21$‰, $n = 100$; data compiled in Stüeken et al., 2015b), likely reflecting minor fractionation during non-quantitative reduction. The fact that only slight isotopic depletion is observed in these bulk marine sediments – in contrast to the large isotopic effects (up to several per mille) seen in laboratory settings (Johnson and Bullen, 2004) – may partly derive from dilution of the isotopically depleted signal (which is likely retained in the elemental and/or sulfide phase) by unfractionated Se in the organic phase (Stüeken et al., 2015b; Mitchell et al., 2016). Phase-specific Se recovery has been explored in a number of studies (Martens and Suarez, 1997; Kulp and Pratt, 2004; Clark and Johnson, 2010; Fan et al., 2011; Schilling et al., 2011, 2014; Stüeken et al., 2015c), but isotopic data on specific phases in marine sedimentary rocks are limited to a single sample from a study of end-Permian shales (Stüeken et al., 2015c) and three measurements of a weathered outcrop of the Cretaceous Mancos Shale (Clark and Johnson, 2010). These studies indeed found elemental and sulfide-hosted Se to be isotopically depleted relative to bulk rock values, and that Se associated with recalcitrant organic matter comprised the dominant host phase, with an isotopic composition similar to that of the bulk rock (Clark and Johnson, 2010; Stüeken et al., 2015c). Other phase-specific concentration measurements (Kulp and Pratt, 2004) have also shown that organic matter is typically the dominant Se host phase in ancient marine sediments, which suggests that it could mask larger isotopic variability that is preserved in the Se^0 and pyrite phases.

In contrast to settings with non-quantitative reduction, strongly anoxic and/or restricted basins with complete reduction of dissolved Se oxyanions will not fractionate Se isotopes during burial. This causes the underlying marine sediments to approximately record the isotopic composition of aqueous Se in that basin, allowing black shales deposited in these settings to be used to infer the Se isotopic composition of overlying waters. This is conceptually anal-

Please cite this article in press as: Kipp M. A., et al. Basinal hydrographic and redox controls on selenium enrichment and isotopic composition in Paleozoic black shales. *Geochim. Cosmochim. Acta* (2020), https://doi.org/10.1016/j.gca.2019.12.016

ogous to using strongly euxinic facies characterized by quantitative Mo scavenging to estimate the Mo-isotopic composition of contemporaneous seawater (*e.g.*, Gordon et al., 2009). However, in the case of Se, (a) quantitative reduction is thought to be possible under anoxic – and not strictly euxinic – conditions (Oremland et al., 1989; Rue et al., 1997), and (b) the recorded isotopic ratio may not be representative of the global ocean due to the shorter marine residence time of Se (10^3–10^4 yr) than Mo (>10^5 yr; Morford and Emerson, 1999). Black Sea sediments yielded a $\delta^{82/78}$Se composition (avg. + 0.2 ± 0.1‰, $n = 12$; Mitchell et al., 2012) that is thought to record quantitative scavenging of aqueous Se from the overlying watermass, whose $\delta^{82/78}$Se composition is therefore not substantially offset from that of the open ocean. However, the effects of basinal restriction and hydrography on Se isotope signatures remain unexplored in ancient settings. In the present study, we evaluate these effects using proxies for watermass exchange with the open ocean.

2.3. Evolution of the global selenium cycle

Although modern marine Se cycling involves a large, oxic reservoir of Se oxyanions with reductive immobilization limited to porewaters or volumetrically-limited anoxic water columns, this does not describe the operation of the Se cycle in deep time prior to the oxygenation of the atmosphere and ocean. In Archean sediments deposited before the Great Oxidation Event (GOE), Se abundances and isotopic fractionations are typically small – likely owing to limited oxidative weathering and efficient, quantitative oxyanion reduction in strongly anoxic oceans (Stüeken et al., 2015b). Notable exceptions occur during transient pulses of oceanic and atmospheric oxygenation wherein Se was evidently mobilized at higher rates and accumulated to higher concentrations in mildly oxic surface waters (Stüeken et al., 2015a; Koehler et al., 2018). The Se cycle was substantially perturbed by the GOE, with a significant increase in Se abundance in marine sediments and marked isotopic fractionation suggesting non-quantitative reduction in suboxic shallow waters (Kipp et al., 2017). The hypothesized mid-Proterozoic interval of reduced atmospheric pO_2 is marked by muted Se abundances and isotopic variability (Stüeken et al., 2015b), followed by large isotopic excursions associated with the Neoproterozoic "Snowball Earth" glaciations that are thought to indicate progressive ocean oxygenation (Pogge von Strandmann et al., 2015). Following their first appearance in the Neoproterozoic, isotopically depleted marine sediments became more common in the Phanerozoic as well-oxygenated oceans with a large Se oxyanion reservoir and non-quantitative reduction became established (Stüeken et al., 2015b).

The units considered in the present study were deposited after deep-ocean oxygenation is thought to have occurred (Dahl et al., 2010; Chen et al., 2015; see review in Qie et al., 2019). This implies that a sizable Se oxyanion reservoir would have been available in open-marine settings, with any deviations from this signal likely attributable to local basinal restriction and redox chemistry rather than global secular changes in the marine oxygen inventory. We used a variety of major and trace elemental proxies to account for these potential local effects on Se abundance and isotopic fractionation in a range of black shales deposited in the late Paleozoic.

3. MATERIALS

3.1. Late Pennsylvanian: North American Midcontinent Sea

3.1.1. Paleogeographic context

The samples utilized in this study come from two intervals of deposition on the North American craton in the late Paleozoic Era. The first interval we consider is the Late Pennsylvanian, during which time the North American Midcontinent Sea (NAMS) spread across the Laurentian Craton (Fig. 2A) at times of glacioeustatic highstand (Heckel, 1977, 1994; Algeo and Heckel, 2008). Marine waters were supplied to the NAMS from oxygen-depleted intermediate depths of the eastern tropical Panthalassic Ocean (ETPO) (Algeo et al., 2008a, 2008b), which, in combination with terrestrial freshwater influx from surrounding mountains (indicated by depletion in carbonate δ^{18}O values; Joachimski and Lambert, 2015; Roark et al., 2017; Jimenez et al., 2019), led to a "superestuarine" circulation pattern in which oxygen-depleted marine waters underlay a reduced-salinity (probably brackish) surface layer (Algeo et al., 2008a, 2008b; Turner et al., 2019). Thick and laterally extensive organic-rich shales were deposited beneath these anoxic deep waters and are preserved across much of the midcontinent United States (Heckel, 1977, 1994; Algeo and Heckel, 2008).

The NAMS was separated into distinct basins by submarine structural highs, which prevented exchange of bottom waters (Heckel, 1977). The largest of these was the Mississippi River Arch, which divided the Midcontinent Shelf from the Illinois Basin (Fig. 2A) (Algeo and Herrmann, 2018). Spatial variation in sediment geochemistry across the NAMS has been used to identify lateral gradients in watermass chemistry (Herrmann et al., 2015, 2019) and sources of detrital siliciclastic material from the Laurentian Craton, Alleghenian Mountains, and Ouachita Mountains (Turner et al., 2019). The influx of terrigenous material and freshwater from these regions led to a counter-clockwise gyral surface circulation pattern (Turner et al., 2019), moving surface waters toward the Panhandle Strait, *i.e.*, the narrow corridor that connected the southwestern corner of the NAMS to the Midland Basin and Hovey Channel and thence to the ETPO (Algeo et al., 2008a, 2008b; Fig. 2A).

3.1.2. Stratigraphic context of drillcores

In this study, we utilized four organic-rich black shale units from three drillcores from the NAMS (Fig. 2A; Table 1). The Tacket Shale (lateral equivalent of the Hushpuckney Shale; cf. Algeo and Maynard, 2004; Cruse and Lyons, 2004) was investigated in drillcore C-TW-1 from the Oklahoma Geological Survey (cf. Cruse and Lyons, 2004; Algeo and Herrmann, 2018). The Stark and Muncie Creek shales of the Kansas City Group were investigated

Please cite this article in press as: Kipp M. A., et al. Basinal hydrographic and redox controls on selenium enrichment and isotopic composition in Paleozoic black shales. *Geochim. Cosmochim. Acta* (2020), https://doi.org/10.1016/j.gca.2019.12.016

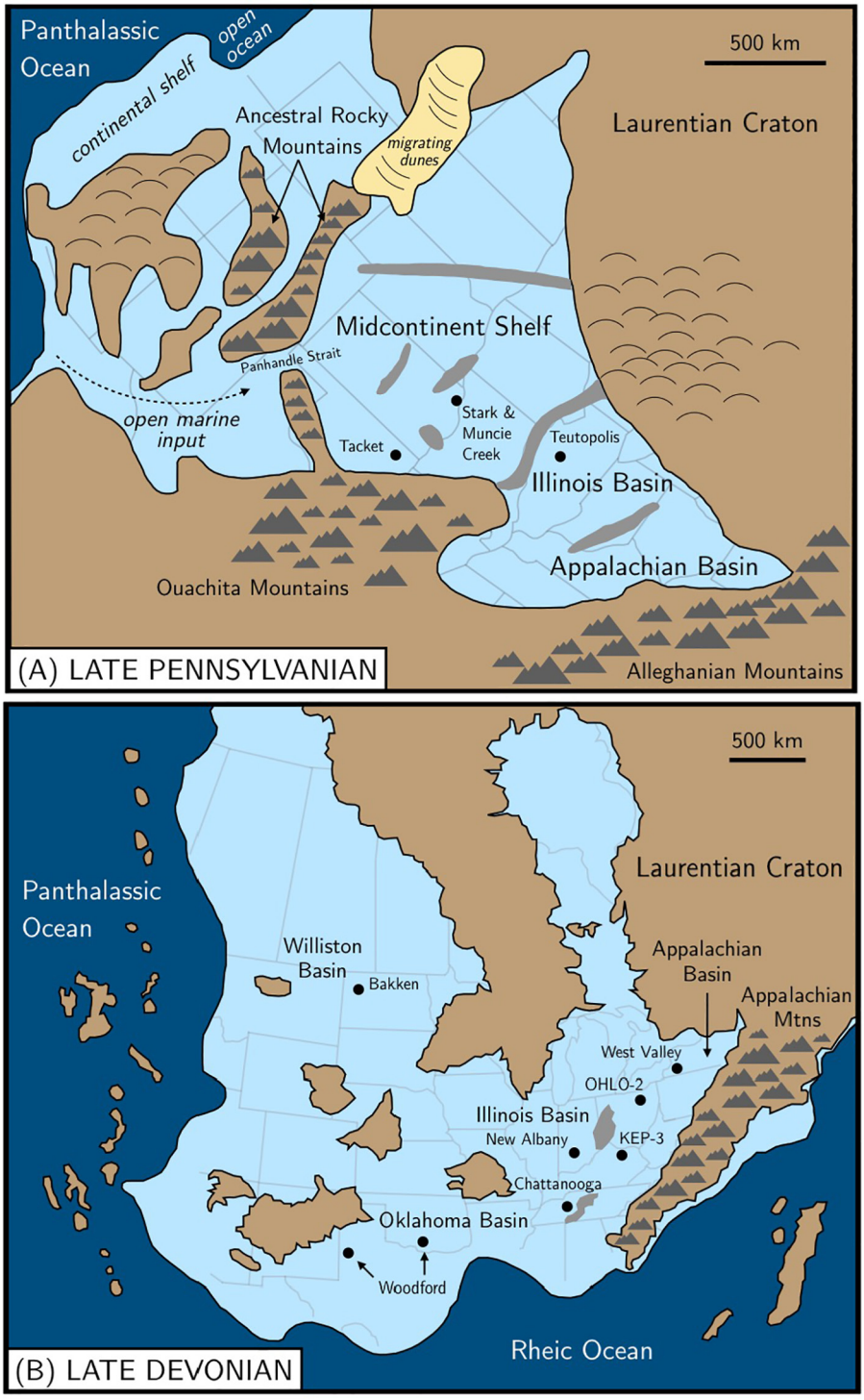

Fig. 2. **Paleogeographic reconstruction of North America in the (A) Late Pennsylvanian and (B) Late Devonian.** All sample sites are denoted with labeled points. Grey bands denote submarine topographic highs separating basins. Maps were modified from Turner et al. (2019) and Algeo et al. (2007), respectively.

in the Edmonds #1A core from the Kansas Geological Survey (cf. Algeo and Maynard, 2004, 2008). The Teutopolis Shale of the Mattoon Formation (lateral equivalent of the Heebner Shale; cf. Turner et al., 2019) was investigated in the Englebart core from the Illinois Geological Survey. The Tacket, Stark, and Muncie Creek shales belong to the Missourian Stage, and the Teutopolis Shale to the Virgilian Stage of the North American Upper Pennsylvanian.

The three study sites represent a gradient in their proximity to marine source waters. The Tacket Shale was

Please cite this article in press as: Kipp M. A., et al. Basinal hydrographic and redox controls on selenium enrichment and isotopic composition in Paleozoic black shales. *Geochim. Cosmochim. Acta* (2020), https://doi.org/10.1016/j.gca.2019.12.016

Table 1
Location information for the 10 study sections.

Section	Unit	Location	Curation[a]
C-TW-1	Tacket	Tulsa Co., OK: T22N, R13E, Sec. 6 SE-NE-NE-SW-SE; 36.416°N, 95.957°W	Oklahoma GS
KGS Edmonds #1A (ED)	Stark	Leavenworth Co., KS: T9S, R22E, Sec. 35 SE-SE-NW-SW; 39.220°N, 94.933°W	Kansas GS
KGS Edmonds #1A (ED)	Muncie Creek	Leavenworth Co., KS: T9S, R22E, Sec. 35 SE-SE-NW-SW; 39.220°N, 94.933°W	Kansas GS
ISGS #1 Englebart (EB)	Teutopolis	Jasper Co., IL: 40′ FSL, 340′ FEL, Sec. 9, T8N, R8E; 39.146°N, 88.318°W; elev. 575′	Illinois GS
Western New York Nuclear Fuel Service #1 [NX-1], also "West Valley core" (WVC)	Hanover-Dunkirk	Cattaraugus County, NY (42.4457°N, 78.6344°W)	New York GS
OHLO-2	Cleveland Member, Ohio Shale	Loraine County, OH (41.4001°N, 82.2438°W, elev. 683 ft)	Ohio GS
KEP-3	Cleveland Member, Ohio Shale	Lewis County, KY (38.409°N, 83.437°W)	Kentucky GS
Dupont HGS (DHGS)	Chattanooga	Humphreys County, TN (36.075°N, 87.495°W)	Tennessee GS
Ryan Shale Pit (RSP)	Woodford	Pontotoc County, OK (34.674°N, 96.641°W)	outcrop
Classen Lake YMCA (CLY)	Woodford	Murray County, OK (34.46°N, 97.15°W)	outcrop
Amoco A.J. Davis #9 (AJD)	Woodford	Yoakum County, TX (33.14°N, 102.89°W)Block D, Sec. 514, 2173 FSL, 1430 FEL; elev. 3710′; J.H. Gibson survey	Texas BEG
Thompson	Upper Bakken	Billings County, ND (47.229 °N, 103.263 °W)	North Dakota GS

[a] GS = Geological Survey; BEG = Bureau of Economic Geology.

deposited nearest to the influx of marine waters through the Panhandle Strait, whereas the Stark and Muncie Creek shales were deposited toward the center of the Midcontinent Shelf (see Algeo et al., 2008a, their Fig. 5). The Teutopolis Shale was deposited in the Illinois Basin and so is likely to have experienced different bottom-water conditions due to lack of deep-water communication between the Illinois Basin and Midcontinent Shelf (Algeo and Herrmann, 2018). This hydrographic separation figures into our interpretation of controls on Se enrichment and isotopic variability between these units.

3.2. Late Devonian: North American Seaway

3.2.1. Paleogeographic context

The second interval considered in this study is the Late Devonian (and earliest Carboniferous at one locality; see below), when organic-rich black shales were widely deposited in multiple basins across the North American continent (Fig. 2B) in what is referred to as the North American Seaway (NAS) (Algeo et al., 2007). The basins within the NAS were typically silled and thus had limited bottom-water exchange with adjacent basins or the open ocean, although the degree of restriction was variable from basin to basin (Algeo et al., 2007). This variation in watermass restriction provides a basis for interpretation of variability in Se abundance levels and isotopic compositions in the study units.

The easternmost of the black shale successions is from the Appalachian Basin. The oldest strata are found in the northern part of the basin, dating to the Middle Devonian with deposition of the Esopus and Needmore shales, followed by the Marcellus Group, Hamilton Group, and Geneseo through Dunkirk shales of early Late Devonian age (Werne et al., 2002; Sageman et al., 2003; Lash, 2017). The central and southern portions of the Appalachian Basin host younger black shale successions, with deposition commencing in the Late Devonian, including the Ohio and Sunbury shales in the central Appalachian Basin and the Chattanooga Shale further south (Algeo et al., 2007). To the west, the Illinois Basin hosts Middle and Upper Devonian shales broadly assigned to the New Albany Shale (or New Albany Group) (*e.g.*, Lineback, 1970). There, deposition commenced in the Middle Devonian with the Portwood and lower Blocher members, followed by the upper Blocher, Selmier, Morgan Trail, Camp Run and Clegg Creek members in the Late Devonian (Algeo et al., 2007). Still further west, widespread black shales across the central to southern Midcontinent region are assigned to the Woodford Formation (Over, 1992, 2002), which is up to ~200 m thick in places and of Late Devonian age. To the north, uppermost Devonian and lowermost Carboniferous black shales of the Bakken Formation were deposited in the Williston Basin of North Dakota, Montana, and southern Alberta, and its lateral equivalent, the Exshaw Formation, was deposited in the Elk Point Basin of central and northern Alberta.

3.2.2. Stratigraphic context of drillcores

In this study, we analyzed black shale samples from eight sites representing multiple formations in several basins of the NAS (Table 1). This approach allowed us to evaluate Se concentrations and isotopic compositions in basins showing varying degrees of watermass restriction, from relatively weaker restriction along the southern mar-

Please cite this article in press as: Kipp M. A., et al. Basinal hydrographic and redox controls on selenium enrichment and isotopic composition in Paleozoic black shales. *Geochim. Cosmochim. Acta* (2020), https://doi.org/10.1016/j.gca.2019.12.016

gin of the NAS (*e.g.*, Oklahoma Basin) to relatively stronger restriction in craton-interior areas (*e.g.*, Illinois and Williston basins). The large Appalachian Basin, which extended from its silled southern margin in Tennessee > 1000 km northward to the Catskill Delta complex in New York, is known to have exhibited internal lateral gradients in sediment chemistry and watermass properties (Algeo et al., 2007; Algeo and Tribovillard, 2009). These environmental conditions contributed to development of pervasive fine-scale (dm-thick) compositional cyclicity throughout this black shale succession.

In the northern Appalachian Basin, we analyzed the black shale succession of the Hanover and Dunkirk Formations in the West Valley core from western New York state (cf. Sageman et al., 2003; Ver Straeten et al., 2011). In the central Appalachian Basin, we analyzed the Cleveland Member of the Ohio Shale in the OHLO-2 core from northern Ohio and the KEP-3 core from northern Kentucky (cf. Jaminski, 1997; Jaminski et al., 1998). In the southern Appalachian Basin, we sampled the Chattanooga Shale in the Dupont HGS drillcore from northern Tennessee (cf. Over et al., 2019). In the Oklahoma Basin, we analyzed the Woodford Formation at three sites: the Ryan Shale Pit (RSP) and Classen Lake area YMCA (CLY) outcrops in south-central Oklahoma (cf. Over, 1992, 2002) and the Amoco A.J. Davis #9 (AJD) drillcore from Yoakum County, Texas. In the Williston Basin, we sampled the Upper Bakken Shale in the Texaco Thompson #5–1 core from Billings County, North Dakota (cf. Hartwell, 1998). We additionally compiled published Se concentration and isotopic data from the Camp Run member of the New Albany Shale (Mitchell et al., 2012). All of the sampled units listed above date to the Late Devonian (Frasnian-Famennian stages), with the exception of the Upper Bakken Shale, which was deposited in the earliest Mississippian.

4. METHODS

4.1. Selenium measurements

Samples were prepared for Se isotope analysis following published protocols (Stüeken et al., 2013). Homogenized rock powders were dissolved in a mixture of concentrated HF, concentrated $HClO_4$, and 8 M HNO_3 at 130 °C. Digests were then evaporated to incipient dryness and additional $HClO_4$ was added to ensure complete oxidation of recalcitrant organic matter. The final digests were evaporated to incipient dryness, 6 M HCl was added, and beakers were placed in a boiling water bath for at least 30 minutes in order to reduce all Se^{VI} to Se^{IV}. Solutions were then diluted to 0.6 M HCl and run through thiol cotton fiber (TCF) columns for separation of Se. Following column chemistry, Se was liberated from the TCF by adding concentrated HNO_3 to the resin in test tubes, which were then placed in a boiling water bath for 20 minutes. Selenium was recovered from the solution in weak HNO_3 via centrifugation. The weak HNO_3 solution was evaporated down to 0.5 mL at 55 °C, at which point aqua regia (3:1 HCl: HNO_3) was added to the sample to remove germanium (Stüeken et al., 2013). The aqua regia solution was also evaporated down to 0.5 mL, at which point the sample was re-dissolved in 6 M HCl and boiled in a water bath for 30 minutes to ensure quantitative reduction to Se^{IV}. The final sample solution was diluted to 0.6 M HCl for analysis.

The measurement of Se concentrations and isotope ratios was conducted on a Nu Plasma Multicollector Inductively Coupled Plasma Mass Spectrometer (MC-ICP-MS) in the Isotope Geochemistry Laboratory at University of Washington following analytical protocols described by Stüeken et al. (2013). Sample solutions were introduced to the MC-ICP-MS via a hydride generator (HG). Sample solutions were mixed in the HG with a 1% $NaBH_4$ solution to catalyze the reduction of Se^{IV} to Se^{-II} (in the form of H_2Se), which was then carried across a teflon membrane and into the MC-ICP-MS via argon (Ar) carrier gas.

Lens voltage potentials, position of the plasma torch, and carrier gas flow rate were tuned daily to optimize signal strength and stability. Measurements were normalized using standard-sample bracketing with the Se NIST SRM 3149 solution (cf. Carignan and Wen, 2007) as the bracketing standard. Isobaric interferences deriving from Ar species were corrected following the method of Stüeken et al. (2013); other isobaric interferences were negligible within analytical precision and so were not corrected. All isotopic data are reported in delta notation relative to NIST reference SRM 3149. We report isotopic data as $\delta^{82/78}Se$ values because this isotopic pair is the least affected by isobaric interferences under our analytical protocol. We note that many other studies (*e.g.*, Chang et al., 2017; Mitchell et al., 2012, 2016; Pogge von Strandmann et al., 2015; Schilling et al., 2011) report Se isotopic data as $\delta^{82/76}Se$ values; these ratios can be converted to $\delta^{82/78}Se$ if it is assumed that Se isotopic fractionation is mass-dependent (cf. Stüeken et al., 2013, 2015b; Pogge von Strandmann et al., 2014).

The external reproducibility of $\delta^{82/78}Se$ measurements was $\pm$ 0.36‰ (2σ), determined by replicate digestions and analyses ($n = 11$) of in-house standard UW-McRae over a period of six months. The average internal uncertainty (2 SE, *i.e.* 95% confidence interval) of replicate sample analyses was ±0.25‰. Samples were analyzed in replicate whenever possible; all isotopic data are reported with 95% confidence intervals unless stated otherwise. Isotopic data obtained for in-house standard UW-McRae and USGS standard SGR-1 were $+0.91 \pm 0.10$‰ ($n = 11$, separate digests) and -0.14 ± 0.28‰ ($n = 4$, separate digests), respectively, which are in agreement with previous studies (Mitchell et al., 2012; Stüeken et al., 2013, 2015b; Kurzawa et al., 2017; Kipp et al., 2017; Pogge von Strandmann et al., 2014, 2015; Schilling et al., 2011). Uncertainty for Se concentration measurements was ±7% (RSD).

4.2. Published data compilation

Additional major and trace element data were compiled from published studies to supplement the Se data generated in this study. Where additional data had not been pub-

lished, we made measurements following the protocols described below. All data that form the basis of conclusions drawn in this paper are reported in Tables 2–4 with corresponding references to original studies in the cases of compiled data.

4.3. Organic carbon and nitrogen measurements

The concentration and isotopic composition of total nitrogen and organic carbon were measured on decarbonated powders following published protocols (Kipp et al., 2018). Bulk rock powders were treated with two overnight iterations of 6 M HCl to dissolve all carbonate phases. De-carbonated powders were then rinsed with 18 MΩ DI-H_2O and dried in an oven at 60 °C. The dried powders were weighed into tin cups for analysis. Total nitrogen (TN), total organic carbon (TOC), and the isotopic composition of bulk nitrogen ($\delta^{15}N$) and organic carbon ($\delta^{13}C$) were measured on single aliquots of decarbonated powder on a Costech™ ECS 4010 Elemental Analyzer coupled to a ThermoFinnigan™ MAT253 continuous flow isotope ratio mass spectrometer housed in IsoLab at the Department of Earth and Space Sciences, University of Washington. Combustion was carried out at 1000 °C. The sample gases were carried through a reduced copper column to reduce NO_x species to N_2 and scrub excess O_2 from the gas stream. A magnesium perchlorate trap was then used to remove water from the gas stream. Raw data were corrected using a two-point calibration (Coplen et al., 2006) with three in-house standards: two glutamic acids (GA1, TOC = 40.8%, TN = 9.5%, $\delta^{13}C = -28.3‰$, $\delta^{15}N = -4.6‰$; GA2, TOC = 40.8, TN = 9.5, $\delta^{13}C = -13.7‰$, $\delta^{15}N = -5.7‰$) and dried salmon (SA, TOC = 45.7%, TN = 11.8%, $\delta^{13}C = -21.3‰$, $\delta^{15}N = +11.3‰$), which are calibrated to international reference materials USGS-40 and USGS-41 and were analyzed four times each per analytical session. Isotopic data are reported in delta notation relative to air for nitrogen and Vienna Pee Dee Belemnite (VPDB) for carbon. Analytical blanks resulting from combustion were measured and subtracted from nitrogen data; analytical blanks were below detection limits for carbon. The external reproducibility (1σ) of isotopic measurements across all runs, as determined by replicate analyses of in-house standard UW-McRae ($\delta^{15}N = +5.6‰$, $\delta^{13}C_{org} = -37.4‰$), was ±0.3‰ for $\delta^{15}N$ and ±0.1‰ for $\delta^{13}C$. Average precision (RSD) of concentration measurements was ±2% for TN and ±0.5% for TOC.

4.4. Total sulfur measurements

For total sulfur (TS) analysis, bulk rock powders were weighed into tin cups along with V_2O_5 as a combustion aid. Measurements were conducted using a Eurovector Elemental Analyzer coupled to a ThermoFinnigan™ MAT253 continuous flow isotope ratio mass spectrometer housed in IsoLab at the Department of Earth and Space Sciences, University of Washington. Combustion was carried out at 1050 °C. The combustion products were carried through a magnesium perchlorate trap to remove oxygen from the gas stream, followed by an 850 °C quartz chip column to allow complete equilibration of oxygen isotopes in the resulting SO_2 with oxygen in the quartz chips (Fry et al., 2002). Raw data were corrected using a two-point calibration with three in-house standards: zinc sulfide (ZnS, TS = 32.9%) silver sulfide (Ag_2S, TS = 12.9%) and barium sulfate ($BaSO_4$, TS = 13.7%), which are calibrated to international reference material IAEA-S-1 and were analyzed three times each per analytical session. The average precision of TS measurements, as determined by replicate analyses of in-house standard $BaSO_4$, was ±2% (RSD).

4.5. Statistical analyses

Linear and logarithmic regression were used to assess the relationships between various geochemical data within and among units (see Results). Data binned across the NAMS and NAS sample sets were compared using the Wilcoxon rank sum tests due to rejection of the null hypothesis in the Shapiro-Wilk normality test for all parameters.

5. RESULTS

All new and compiled data for the Upper Pennsylvanian black shales of the NAMS are presented in Table 2. Selenium isotope ratios in this dataset range from −1.15‰ to +0.77‰, with unit averages showing > 1‰ variation, *i.e.*, Muncie Creek = +0.50 ± 0.21‰ ($n = 5$), Tacket = −0.01 ± 0.28‰ ($n = 7$), Stark = −0.13 ± 0.38‰ ($n = 6$), and Teutopolis = −0.55 ± 0.25‰ ($n = 7$). Selenium concentrations range from 0.3 to 135.5 μg/g. Selenium enrichment factors (EF), calculated following the approach of Tribovillard et al. (2006), and with the same crustal Se/Al ratio (Se/Al = 17.4 μg/g) that has been used in recent deep-time Se studies (Stüeken et al., 2015a; Koehler et al., 2018), range from 1.7 to 1465. Across all NAMS samples, $\delta^{82/78}Se$ values positively correlate with TOC (wt. %) ($p < 0.01$; $R^2 = 0.60$, linear regression) as well as Se (EF) ($p < 0.01$; $R^2 = 0.41$, linear regression) (Fig. 3).

No statistically significant correlations are observed between unit average $\delta^{82/78}Se$ values and proxies for redox or hydrographic conditions for the four Upper Pennsylvanian study units (Fig. 3). Nitrogen isotope ratios are nearly invariant (unit means range from +5.5‰ to +7.2‰) and do not correlate with $\delta^{82/78}Se$ values ($p = 0.89$). Fe/Al (g/g) ratios do not correlate with $\delta^{82/78}Se$ values ($p = 0.89$) and are similar in all units except the Tacket Shale, which is more Fe-rich. Similarly, DOP_T (the degree of pyritization as estimated from total S and Fe contents; Algeo et al., 2008b) is highest in the Tacket Shale, and across all units DOP_T is not correlated with $\delta^{82/78}Se$ values ($p = 0.78$). Moderate differences between units are observed in average Mo/TOC ratios, which range from ~3 to 10 (10^4 * g/g), but this variability is not correlated with $\delta^{82/78}Se$ values ($p = 0.55$). Mean Sr/Ba ratios of individual units range from 0.5 to 1.0 (g/g) and do not correlate with $\delta^{82/78}Se$ values ($p = 0.88$).

In contrast to the lack of relationships with unit average values, individual data points within certain units show significant correlations between Se concentrations (μg/g) and enrichment factors (EF) and other geochemical proxies.

Please cite this article in press as: Kipp M. A., et al. Basinal hydrographic and redox controls on selenium enrichment and isotopic composition in Paleozoic black shales. *Geochim. Cosmochim. Acta* (2020), https://doi.org/10.1016/j.gca.2019.12.016

Table 2
Geochemical data from late Pennsylvanian shales. Published data cited in footnotes.

Unit	Sample ID	Se (μg/g)	$\delta^{82/78}$Se (‰)	$\delta^{82/78}$Se (95% CI)	TOC (wt. %)	TS (wt. %)	δ^{15}N (‰)	Al (wt. %)	Fe (wt. %)	Mo (μg/g)	DOP_T
Muncie Creek	EDM 27-9	67.6	0.77	0.37	14.01[a]	1.16[a]	6.7[b]	7.62[a]	3.84[a]	71.56[a]	0.26[a]
Muncie Creek	DMB-10	81.1	0.64	0.11	16.87[a]	1.17[a]	6.5[b]	7.06[a]	3.98[a]	82.85[a]	0.26[a]
Muncie Creek	DMB-50	43.2	0.57	0.27	19.23[a]	0.89[a]	5.2[b]	6.94[a]	3.67[a]	40.06[a]	0.21[a]
Muncie Creek	DMB-60	38.8	0.22	0.28	18.54[a]	1.32[a]	4.4[b]	8.05[a]	3.95[a]	30.96[a]	0.29[a]
Muncie Creek	DMB-73	64.7	0.29	0.01	9.26[a]	2.90[a]	4.6[b]	8.58[a]	5.41[a]	31.87[a]	0.47[a]
Stark	S-ED-X4	86.9	0.62	0.24	13.18[a]	1.70[a]	6.8	6.22[a]	3.29[a]	655.71[a]	0.45[a]
Stark	S-ED-X26	18.2	−0.11	0.26	6.54[a]	1.39[a]	5.6[b]	8.56[a]	3.86[a]	7.89[a]	0.31[a]
Stark	S-ED-X28	16.3	−0.03	0.11	6.41[a]	1.47[a]	6.0[b]	8.58[a]	3.86[a]	6.87[a]	0.33[a]
Stark	S-ED-X31	13.5	−0.07	0.34	4.40[a]	1.87[a]	5.7[b]	8.58[a]	4.37[a]	5.33[a]	0.37[a]
Stark	S-ED-X32	10.4	−0.42	0.37	4.08[a]	1.73[a]	5.7[b]	8.70[a]	4.03[a]	3.26[a]	0.37[a]
Stark	S-ED-X33	10.7	−0.78	0.26	2.09[a]	2.25[a]	6.1[b]	8.76[a]	4.54[a]	3.53[a]	0.43[a]
Tacket	275.2	0.3	0.03		0.91[c]	0.22[c]	4.7	9.48[c]	6.99[c]	1.12[c]	0.03[c]
Tacket	216–222	41.9	0.03	0.18	9.45[c]	8.78[c]	6.1	6.47[c]	6.77[c]	14.10[c]	0.97[c]
Tacket	202.5–205.0	33.6	−0.15	0.15	15.51[c]	10.92[c]	5.6	2.97[c]	7.33[c]	21.96[c]	1.00[c]
Tacket	174.0–176.3	110.8	0.33	0.25	18.51[c]	8.87[c]	5.8	5.00[c]	6.68[c]	65.89[c]	1.00[c]
Tacket	132.0–134.5	135.5	0.46	0.19	18.71[c]	4.79[c]	14.1	5.31[c]	4.70[c]	186.89[c]	0.89[c]
Tacket	84.5–87.5	6.6	−0.68	0.11	1.01[c]	3.46[c]	7.5	6.18[c]	3.89[c]	18.42[c]	0.78[c]
Tacket	57	22.9	−0.07	0.11	6.77[c]	1.89[c]	6.5	7.51[c]	3.51[c]	6.29[c]	0.47[c]
Teutopolis	5	0.6	−0.46	0.41	1.28[d]	1.30[d]	5.0	9.32[d]	3.98[d]	1.45[d]	0.28[d]
Teutopolis	15	0.7	−0.55		0.45[d]	1.90[d]	5.0	8.78[d]	3.98[d]	2.39[d]	0.42[d]
Teutopolis	35	1.0	−0.13	0.27	0.47[d]	1.87[d]	5.5	8.50[d]	3.91[d]	4.64[d]	0.42[d]
Teutopolis	45	1.0	−0.69	0.16	0.65[d]	2.31[d]	5.7	8.66[d]	4.06[d]	4.04[d]	0.49[d]
Teutopolis	55	2.2	−1.15	0.17	1.16[d]	2.07[d]	6.0				
Teutopolis	75	20.6	−0.29	0.30	9.89[d]	3.27[d]	6.8	8.40[d]	6.03[d]	24.64[d]	0.47[d]
Teutopolis	91	12.6	−0.58	0.23	4.82[d]	2.50[d]	6.2	7.65[d]	4.5[d]	19.64[d]	0.48[d]

[a] Algeo and Maynard (2004).
[b] Algeo et al. (2008b).
[c] Algeo and Tribovillard (2009).
[d] Turner et al. (2019).

Table 3
Geochemical data from Late Devonian shales. Published data cited in footnotes.

Unit	Sample ID	Se (μg/g)	$\delta^{82/78}$Se (‰)	$\delta^{82/78}$Se (95% CI)	TOC (wt. %)	TS (wt. %)	δ^{15}N (‰)
Dunkirk	WVC754-14	0.7	−0.24	0.75	1.89	2.20	0.6
Dunkirk	WVC754-2-5	0.4	−0.52		0.65	2.69	0.9
Hanover	WVC785-13	0.4	0.02		2.26	2.00	0.2
Hanover	WVC785-8	0.4	0.10		2.64	1.82	−0.5
Woodford	RSP-22	2.6	−0.30	0.35		0.44	
Woodford	RSP-40	8.2	−0.87	0.54		0.79	
Woodford	AJD-507	0.6	−0.36			0.52	
Woodford	AJD-513	1.1	−0.14			0.65	
Woodford	CLY-24	4.9	0.24	0.60		2.22	
Woodford	CLY-26	3.2	0.84	0.18		15.21	
Woodford	CLY-30	1.9	−0.25			1.53	
Woodford	CLY-33	2.4	−0.63	0.07		1.92	
Cleveland Member, Ohio Shale	OHLO-2_540′0′	1.1	1.00		7.94	3.67	0.0
Cleveland Member, Ohio Shale	OHLO-2_530′0′	0.8	0.60		7.02	2.68	−0.4
Cleveland Member, Ohio Shale	OHLO-2_519′9′	1.2	0.81	0.18	7.00	2.11	0.0
Cleveland Member, Ohio Shale	OHLO-2_510′0′	1.2	0.57	0.18	5.24	2.63	0.3
Cleveland Member, Ohio Shale	OHLO-2_469′7′	0.6	0.99		7.20	3.71	−0.3
Cleveland Member, Ohio Shale	OHLO-2_460′0′	0.7	0.75		5.72	5.13	−0.1
Cleveland Member, Ohio Shale	OHLO-2_309′3′	0.8	0.14		4.92	1.76	0.7
Chattanooga	Dup-75	2.2	0.37	0.82	10.36	5.80	1.9
Chattanooga	Dup-64	4.6	−0.38	0.17			
Chattanooga	Dup-54	2.7	1.55				
Chattanooga	Dup-60	2.0	0.93	0.21			
Chattanooga	Dup-33	3.8	−0.66	0.01			
Chattanooga	Dup-15	4.5	−0.06	0.26			
Cleveland Member, Ohio Shale	K3-17-9/2	2.9	0.17	0.25	2.66	2.41	2.0
Cleveland Member, Ohio Shale	K3-17-9/10	2.0	0.50	0.29	6.60	1.35	1.1
Cleveland Member, Ohio Shale	K3-12-8/9	24.3	−0.89	0.21	12.38	8.79	5.0
Cleveland Member, Ohio Shale	K3-12-8/4	37.0	−0.72	0.07	5.57	9.07	4.2
Cleveland Member, Ohio Shale	K3-12-8/3	8.6	0.23	0.14	11.55	1.53	4.6
Cleveland Member, Ohio Shale	K3-12-8/10	17.6	−0.26	0.01	12.84	2.68	5.1
Upper Bakken	T2-6	0.5	−0.04		0.96	3.10[c]	1.5
Upper Bakken	T2-2	0.4	−0.96		0.92	3.40[c]	1.5
Upper Bakken	T2-15	0.3	−0.44		0.60	3.00[c]	1.8
Upper Bakken	T1-7	0.6	0.19		1.24	4.50[c]	1.5
New Albany (anoxic)		0.5[a]	0.91[a]		8.60[b]	3.79[b]	0.2[d]
New Albany (anoxic)		1.1[a]	0.92[a]		8.96[b]	3.48[b]	
New Albany (anoxic)		0.8[a]	1.20[a]		7.17[b]	3.44[b]	−0.1[d]
New Albany (anoxic)		1.1[a]	1.14[a]		7.24[b]	2.32[b]	0.7[d]
New Albany (anoxic)		1.0[a]	1.52[a]		11.83[b]	3.30[b]	−0.1[d]
New Albany (oxic)		0.5[a]	0.47[a]		0.31[b]	0.56[b]	1.5[d]
New Albany (oxic)		1.0[a]	0.45[a]		0.48[b]	1.63[b]	2.2[d]
New Albany (oxic)		0.8[a]	0.64[a]		0.13[b]	1.19[b]	2.9[d]
New Albany (oxic)		0.6[a]	0.48[a]		0.18[b]	0.42[b]	2.6[d]
New Albany (oxic)		0.4[a]	0.19[a]		0.38[b]	1.39[b]	2.9[d]

[a] Mitchell et al. (2012).
[b] Ingall et al. (1993).
[c] Hartwell (1998).
[d] Calvert et al. (1996).

For example, Se concentrations correlate positively with Mo/TOC ($p < 0.01$, $R^2 = 0.31$, logarithmic regression, Fig. 4A) and Se (EF) correlates positively with Mo (EF) ($p < 0.01$, $R^2 = 0.62$, logarithmic regression, Fig. 4B) for the units deposited on the Midcontinent Shelf (Tacket, Stark, Muncie Creek). Within these units, $\delta^{82/78}$Se values are also positively correlated with Se (μg/g) ($p < 0.01$, $R^2 = 0.48$). Note that this excludes the Teutopolis Shale, which was deposited in the Illinois Basin (Fig. 4) and thus was isolated from bottom-water exchange with the Midcontinent Shelf (Algeo and Herrmann, 2018).

All new and compiled data from the eight study units of the Late Devonian NAS are presented in Table 3. Compiled unit average Mo/TOC and Sr/Ba ratios are presented in Table 4. Selenium isotope ratios in these units range from −1.0‰ to +1.55‰, with unit averages showing ~1.4‰ variation: Bakken = −0.31 ± 0.50‰ ($n = 4$), Woodford = −0.18 ± 0.37‰ ($n = 8$),

Please cite this article in press as: Kipp M. A., et al. Basinal hydrographic and redox controls on selenium enrichment and isotopic composition in Paleozoic black shales. *Geochim. Cosmochim. Acta* (2020), https://doi.org/10.1016/j.gca.2019.12.016

Table 4
Unit-average Mo/TOC and Sr/Ba data for Late Devonian units.

Section	Formation	Mo/TOC[a] (10^4 * g/g)	Sr/Ba[b,c] (g/g)
RSP, CLY, AJD	Woodford	23.4 ± 1.7	0.34 ± 0.14
Thompson	Upper Bakken	13.2 ± 1.5	0.29 ± 0.08
WVC	Hanover-Dunkirk	11.6 ± 6.1	0.26 ± 0.05
KEP-3	Cleveland Member, Ohio Shale	13.9 ± 6.9	0.23 ± 0.02
DHGS	Chattanooga	7.0 ± 5.4	0.45 ± 0.09
INJK-13	Camp Run Member, New Albany (oxic)	N/A	0.24 ± 0.06
INJK-13	Camp Run Member, New Albany (anoxic)	4.5 ± 0.5	0.16 ± 0.04

[a] Mo/TOC data from Algeo et al. (2007) except West Valley and Chattanooga (this study) and presented ± 1σ.
[b] Sr/Ba data from Liu and Algeo (2019) except New Albany (Calvert et al., 1996).
[c] Samples with > 5 wt. % $CaCO_3$ were excluded from calculation due to contamination of signal with carbonate-bound Sr.

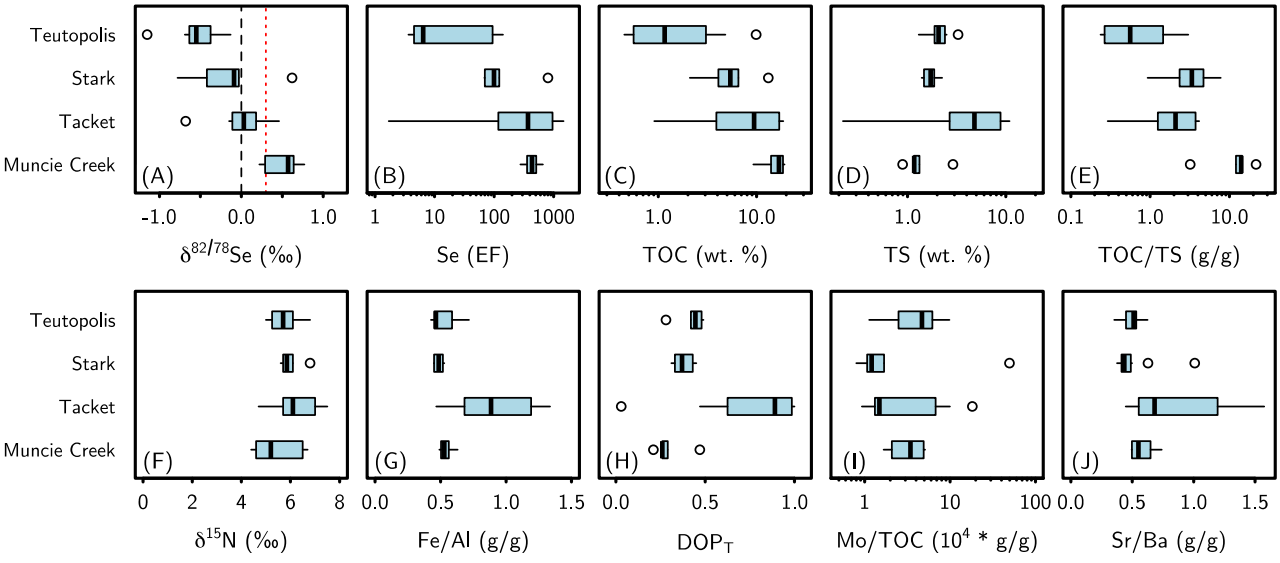

Fig. 3. **Boxplot of (A) $\delta^{82/78}$Se, (B) Se (EF), (C) TOC (wt. %), (D) TS. (wt. %), (E) TOC/TS (wt. %/wt. %), (F) δ^{15}N, (G) Fe/Al (g/g), (H) degree of pyritization (DOP_T), (I) Mo/TOC (10^4 * g/g) and (J) Sr/Ba (g/g) for Late Pennsylvanian units.** In panel A, upper crust composition is denoted with black dashed line; modern seawater composition is noted with red dotted line. The Sr/Ba values for Stark shale were calculated from 11 samples sitting 0–40 cm above the samples measured for Se isotopes. In this and subsequent boxplots, boxes are drawn as the limits of the first and third quartiles, whiskers comprise the 95% confidence interval, and black lines denote the median. (For interpretation of the references to colour in this figure legend, the reader is referred to the web version of this article.)

Hanover-Dunkirk = −0.16 ± 0.28‰ ($n = 4$), Ohio Shale (KEP-3 core) = −0.16 ± 0.46‰ ($n = 6$), Chattanooga = +0.29 ± 0.68‰ ($n = 6$), New Albany (oxic) = +0.45 ± 0.14‰ ($n = 5$), Ohio Shale (OHLO-2 core) = +0.69 ± 0.22‰ ($n = 7$), and New Albany (anoxic) = +1.14 ± 0.22‰ ($n = 5$) (Fig. 5). Se concentrations range from 0.3 to 37.0 μg/g (Fig. 5). Unlike in the NAMS shales, $\delta^{82/78}$Se values are only weakly correlated with TOC/TS ($p < 0.01$, $R^2 = 0.17$, logarithmic regression; Fig. 6A). Also unlike the NAMS shales, $\delta^{82/78}$Se values in the NAS samples are negatively correlated with δ^{15}N values ($p < 0.01$, $R^2 = 0.30$, linear regression; Fig. 6B). Se concentrations are also correlated with δ^{15}N values in the NAS samples ($p < 0.01$, $R^2 = 0.47$, logarithmic regression; Fig. 6C). Unit average $\delta^{82/78}$Se values show a significant negative correlation with Mo/TOC ($p = 0.01$, $R^2 = 0.77$, logarithmic regression) (Fig. 7) for the NAS samples.

Across both datasets as a whole, Se concentrations are significantly higher in the Upper Pennsylvanian NAMS black shales than those from the Upper Devonian NAS ($p < 0.01$; Fig. 8). The NAMS shales also have higher Sr/Ba ratios ($p < 0.01$) and δ^{15}N values ($p < 0.01$) than those from the NAS, but there is no significant difference in TOC ($p = 0.18$) or TS ($p = 0.48$) between the two datasets (Fig. 8).

6. DISCUSSION

6.1. Late Pennsylvanian: Potential causes of isotopic variability among units

The large range of $\delta^{82/78}$Se values (Fig. 3A) observed in black shales of the NAMS (−1.15‰ to +0.77‰) spans much of the range of known Se isotopic variability from the geologic record. Furthermore, Se enrichment factors

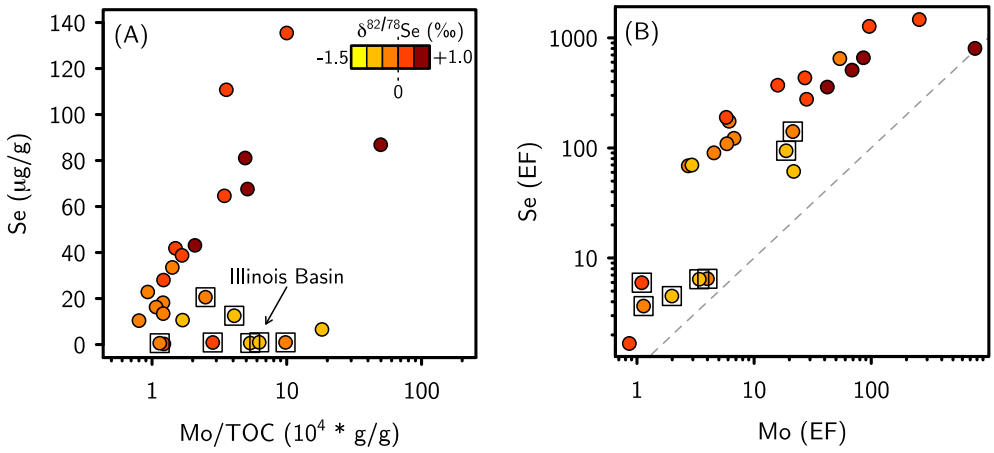

Fig. 4. **Relationship between Se and Mo in Late Pennsylvanian units.** (A) Se (µg/g) vs. Mo/TOC and (B) Se (EF) vs. Mo (EF). Coloration of data points denotes $\delta^{82/78}$Se values, with darker shading indicative of higher values. The positive correlation between Se enrichment and Mo/TOC in units *within* the Midcontinent Shelf environment suggests that the same mechanism was concentrating both trace metals. This is consistent with the nutrient-trap mechanism proposed by Algeo and Herrmann (2018). Furthermore, Se was being enriched relative to Mo by the nutrient trap, as evidenced by higher enrichment factors (EF) across the Midcontinent Shelf. The bottom waters that overlay the Teutopolis Shale in the Illinois Basin were isolated from exchange with the Midcontinent Shelf, thus giving distinct Se (µg/g) vs. Mo/TOC and Se (EF) vs. Mo (EF) trends with smaller Se enrichments.

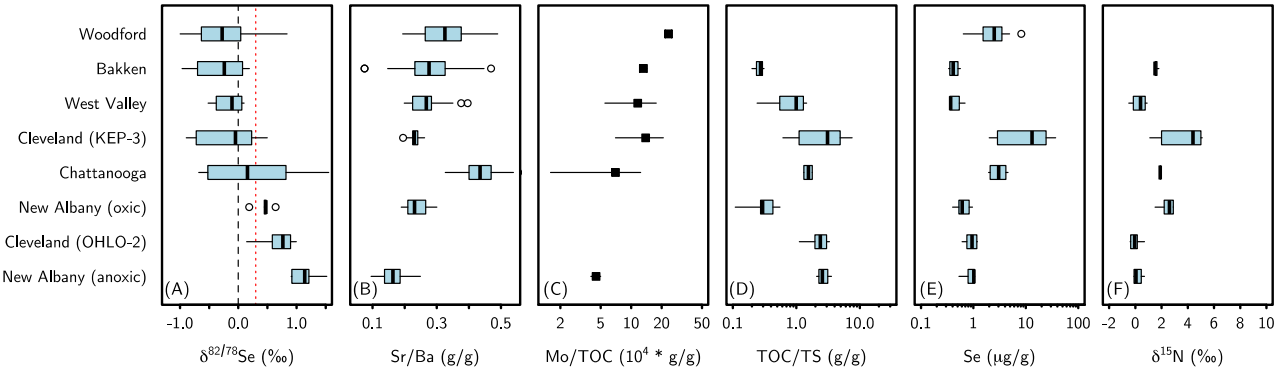

Fig. 5. **Boxplot of (A) $\delta^{82/78}$Se values, (B) Sr/Ba, (C) unit-averaged Mo/TOC, (D) TOC/TS (wt. %/wt. %), (E) Se (µg/g) and (F) δ^{15}N in Late Devonian units.** In panel A, upper crust composition is denoted with black dashed line; modern seawater composition is noted with red dotted line. Unlike in the NAMS black shales, $\delta^{82/78}$Se values do not closely correlate with TOC/TS. On the contrary, Mo/TOC and δ^{15}N show similar trajectories to the $\delta^{82/78}$Se values. (For interpretation of the references to colour in this figure legend, the reader is referred to the web version of this article.)

in the same samples span nearly 3 orders of magnitude (Fig. 3B). Together these data suggest a diversity of Se cycling regimes across these sites. The most positive $\delta^{82/78}$Se values co-occur with the largest Se enrichments (Fig. 3A, B), suggesting that a similar set of mechanisms controlled this covariation.

This wide range of Se enrichments and isotopic ratios conceivably could have arisen from variable redox conditions between the study sites. Specifically, sites with the most reducing bottom waters might be expected to have scavenged Se most efficiently, thereby leading to large Se enrichments and positive $\delta^{82/78}$Se values due to quantitative oxyanion reduction. In contrast, sites with bottom-waters that were suboxic or only transiently anoxic might have experienced non-quantitative Se reduction, thus yielding smaller Se enrichments and more negative $\delta^{82/78}$Se values. However, we do not see compelling evidence for such redox differences between sites.

Bulk-sediment δ^{15}N values are nearly constant across the study sites (Fig. 3F), suggesting that photic zone redox conditions were roughly similar in the different settings. The fact that δ^{15}N values are positive (+4 to +7‰; similar to modern marine sediments, cf. Tesdal et al., 2013) suggests that aerobic nitrogen cycling was occurring and a surface-water nitrate reservoir was present. As nitrate is reduced to N_2 via denitrification at a redox potential similar to that of Se oxyanion reduction (Fig. 1), this would seem to suggest that the upper water column was similarly favorable for Se oxyanion accumulation at each site. We therefore cannot invoke different surface-water redox conditions as a means to explain the variable Se enrichment and isotopic fractionation across the NAMS.

Please cite this article in press as: Kipp M. A., et al. Basinal hydrographic and redox controls on selenium enrichment and isotopic composition in Paleozoic black shales. *Geochim. Cosmochim. Acta* (2020), https://doi.org/10.1016/j.gca.2019.12.016

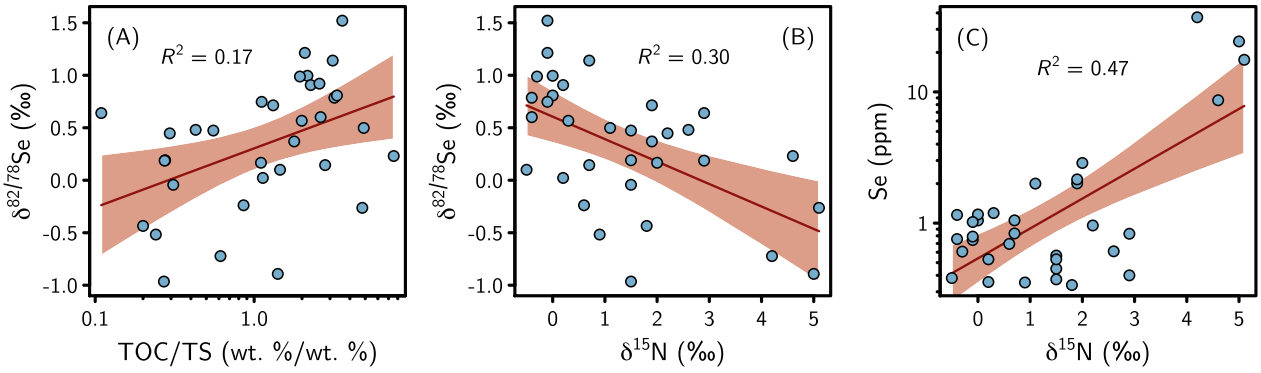

Fig. 6. **Correlation between (A) $\delta^{82/78}$Se and TOC/TS, (B) $\delta^{82/78}$Se and δ^{15}N, and (C) Se (μg/g) and δ^{15}N in Late Devonian units.** The relatively weak correlation between $\delta^{82/78}$Se and TOC/TS suggests that other factors altered the isotopic composition of the organic- and/or sulfide-bound Se fractions. The moderate negative correlation between $\delta^{82/78}$Se and δ^{15}N suggests that some portion of the Se oxyanion pool was being removed at high redox potentials similar to that of nitrate reduction. The muted Se concentrations in settings with near-zero δ^{15}N values suggest that depletion of the nitrate and Se oxyanion reservoirs was indeed concurrent. In contrast, the higher Se concentrations are found in samples with more positive δ^{15}N values, consistent with the presence of nitrate (and Se oxyanions) in the water column.

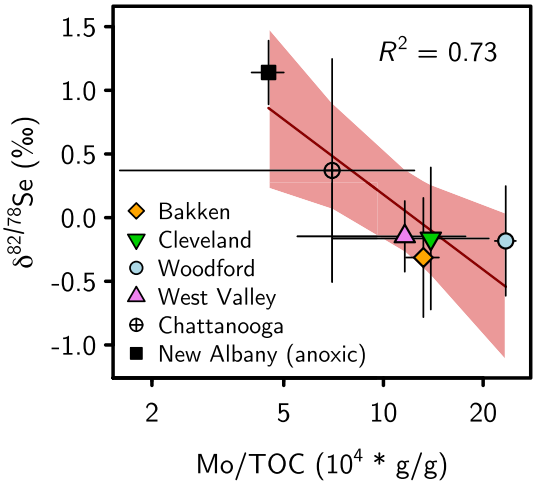

Fig. 7. **Negative correlation between unit-averaged $\delta^{82/78}$Se and Mo/TOC in Late Devonian units.** More negative $\delta^{82/78}$Se values are found in units with higher Mo/TOC ratios, suggesting faster seawater replenishment, which may have enabled non-quantitative Se oxyanion reduction.

Bottom-water redox conditions can be evaluated using Fe geochemistry. The similarities in Fe/Al (Fig. 3G) and DOP_T (Fig. 3H) across study sites – with the exception of the Tacket Shale, which has elevated values likely due to local euxinia (Cruse and Lyons, 2004; Algeo and Herrmann, 2018) – suggest that variable bottom-water redox conditions were not responsible for the observed variations in $\delta^{82/78}$Se or Se (EF). All Fe/Al and DOP_T values are consistent with anoxic deposition across the NAMS, as inferred in earlier studies (Algeo and Maynard, 2004; Algeo and Heckel, 2008); however, we note that these Fe data cannot constrain the depth of the chemocline, which may have been variable across the basin.

If redox was not the dominant control on Se enrichment and isotopic fractionation across the NAMS, another possible mechanism for generating the observed variability in Se cycling is that basinal restriction influenced the size and isotopic composition of the aqueous Se reservoir. In modern anoxic, silled basins, rapid removal of redox-sensitive elements to the sediment without sufficient resupply is known to diminish aqueous Mo concentrations (Algeo and Lyons, 2006), leading to lower sediment Mo/TOC ratios in more strongly restricted settings. We do observe some variability in Mo/TOC ratios across our dataset (Fig. 3I), perhaps suggesting varying degrees of restriction (though this could be confounded by differing degrees of euxinia between sites); however, these trends do not align with Se isotopes or abundances when viewed across all NAMS units. We also compiled Sr/Ba ratios from these samples, as this parameter has recently been proposed as a paleosalinity proxy in shales (Wei et al., 2018; Wei and Algeo, 2019, this issue). Higher Sr/Ba ratios imply greater seawater influence (due to greater Sr concentrations relative to Ba, the latter being effectively scavenged by sulfate in estuarine settings), but we do not observe much variability in Sr/Ba across the study sites. This suggests that variable seawater/freshwater mixing cannot readily account for the observed changes in Se cycling. Such a correlation may not be expected, though, since the average Se concentration in river waters (median $1.1^{+2.2}_{-0.8}$ nM; Conde and Alaejos, 1997) is similar to that of seawater (1–2 nM).

The lack of evidence for strong redox and salinity gradients across the NAMS is consistent with the recent findings of Algeo and Herrmann (2018). Notably, that study identified a large gradient in redox-sensitive trace metal enrichment across the NAMS, with strong enrichments of Mo, U and Zn limited to the most proximal areas of the Midcontinent Shelf. They inferred that this pattern was the result of a nutrient trap akin to that observed in modern estuaries (Shiller, 1996; Audry et al., 2006). In these settings, nutrients and trace metals dissolved in seawater are scavenged in the upper portion of the water column by organic matter (derived from primary production and/or riverine input) and Fe-Mn-oxides (delivered predominantly by rivers). These organic complexes and particulates sink into bottom waters, where trace metals are then released

Please cite this article in press as: Kipp M. A., et al. Basinal hydrographic and redox controls on selenium enrichment and isotopic composition in Paleozoic black shales. *Geochim. Cosmochim. Acta* (2020), https://doi.org/10.1016/j.gca.2019.12.016

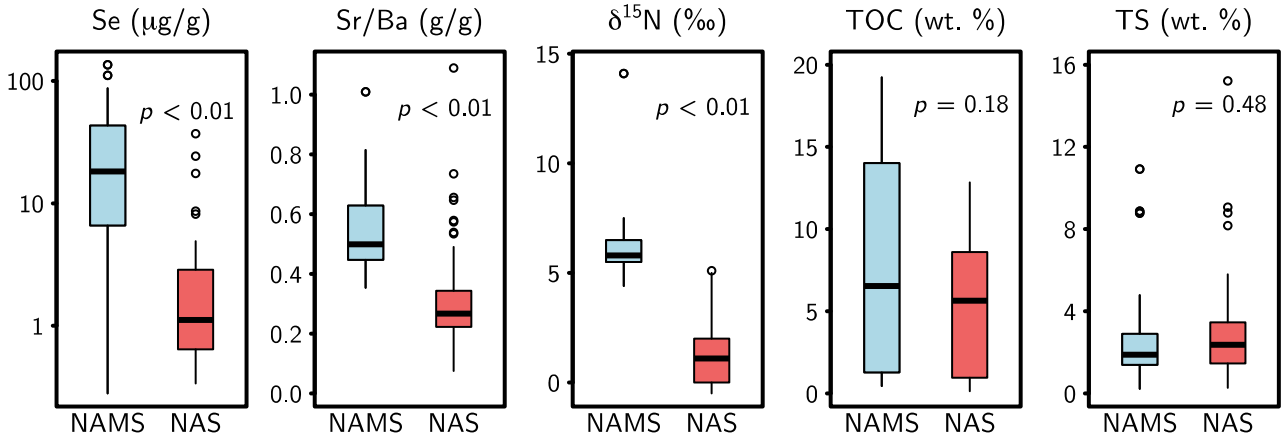

Fig. 8. **Differences in redox, hydrography and Se cycling between the Late Pennsylvanian NAMS and the Late Devonian NAS.** Low Se concentrations in the NAS are likely the result of basinal restriction (evidenced by low Sr/Ba ratios) and Se oxyanion depletion (suggested by low $\delta^{15}N$ values, which imply nitrate depletion). The difference in Se concentrations between the NAMS and NAS is not due to differing TOC or TS contents, suggesting that the controls have to do with watermass circulation and seawater renewal instead of local bottom-water redox conditions.

through reductive dissolution of the host phases. Because bottom waters flow in the landward direction in estuarine circulation systems, this mechanism leads to a progressive concentration of nutrients and trace metals across the most proximal part of the deep watermass, *i.e.*, the "salt wedge" (Algeo and Herrmann, 2018). This process can lead to extreme local enrichments of nutrients and trace metals in sediments. In the case of the NAMS, a sharp drop in trace-metal enrichments between the Midcontinent Shelf and the Illinois Basin to its east was interpreted to represent a lack of deep-water exchange between those areas owing to the physical barrier of the Mississippi River Arch (Algeo and Herrmann, 2018).

Our Se data also seem to be best explained by the nutrient-trap mechanism. Se concentrations in Midcontinent Shelf samples correlate with Mo/TOC ratios (Fig. 4A), suggesting a shared control on the enrichment of these elements. The Teutopolis Shale samples from the Illinois Basin also show a different trajectory with smaller Se enrichments (Fig. 4A), consistent with the isolation of deep waters of the Illinois Basin from the Midcontinent Shelf. The nutrient-trap mechanism can also account for the observed gradient in $\delta^{82/78}Se$ values, with more positive $\delta^{82/78}Se$ values occurring in the most trace-metal-enriched samples (Fig. 4A). One possible explanation for this trend is that non-quantitative Se sequestration in distal sedimentary pore waters of the Midcontinent Shelf preferentially drew lighter Se isotopes into the sediments, enriching the residual aqueous Se reservoir in heavier isotopes, which were then captured via quantitative reduction in the more proximal shelf areas where nutrient trapping was operative. Quantitative reduction in these proximal areas may have been facilitated by high rates of organic matter export to sediments. The lighter $\delta^{82/78}Se$ values in the Teutopolis Shale are indicative of a separate deep-water Se reservoir that was not affected by the enrichment process operating in deep waters of the Midcontinent Shelf.

In this scenario of a nutrient-trap control on Se cycling on the Midcontinent Shelf, organic matter was likely the dominant shuttle for transfer of Se to deep waters. This is indicated by the similar trajectories of Se (EF) and TOC between study units (Fig. 3B, C). In contrast, Se enrichments do not correlate with TS (Fig. 3D), suggesting that Se transfer to the sediment was not controlled by rates of microbial sulfate reduction or pyrite formation. These observations are notable for two reasons. First, it may help to explain why Se is more strongly enriched than Mo in the Midcontinent Shelf samples (Fig. 4B). If substantial organic matter recycling was occurring in the NAMS water column (namely in the more distal portions of the basin), then Se may have been regenerated more efficiently than Mo, which was likely being recycled predominantly via Mn-oxide dissolution in sediment porewaters (and thus was prone to some degree of sequestration via co-precipitation with sulfide minerals). Second, the dominance of total Se by the organic-bound fraction has important implications for bulk rock Se isotopic compositions. As described above, enrichment of proximal bottom waters of the Midcontinent Shelf in heavy Se isotopes could explain the observed trend in $\delta^{82/78}Se$ values.

An alternative possibility is that Se isotopic variability reflects two-component mixing, in which the organic-bound Se^{-II}, sulfide-bound Se^{-II}, and Se^{0} fractions have different $\delta^{82/78}Se$ compositions. The limited phase-specific data available suggest that Se can be present in subequal quantities in organic matter and sulfide minerals (Stüeken et al., 2015c), which is also supported by Se data from phytoplankton biomass (Mitchell et al., 2012) and sedimentary pyrite (Large et al., 2014). Given plausible isotopic compositions (informed by the phase-specific analyses of Stüeken et al., 2015c) for the organic and sulfidic components (*e.g.*, $\delta^{82/78}Se_{organic} = +0.3‰$ to $+1.0‰$ and $\delta^{82/78}Se_{sulfide} = -2.0‰$ to $-1.0‰$), it would be possible to generate the range of observed bulk rock $\delta^{82/78}Se$ compositions in the

Please cite this article in press as: Kipp M. A., et al. Basinal hydrographic and redox controls on selenium enrichment and isotopic composition in Paleozoic black shales. *Geochim. Cosmochim. Acta* (2020), https://doi.org/10.1016/j.gca.2019.12.016

NAMS black shales. In this case, as TOC levels increase, the organic Se fraction would become dominant over the sulfide and Se^0 fractions, leading to higher bulk-rock $\delta^{82/78}Se$ values (*i.e.*, approaching that of the organic-bound Se). We cannot disprove this possibility, but we regard it as secondary to the nutrient-trapping mechanism. The relationship of Se isotopes (Fig. 3A) to TOC (Fig. 3C) is stronger than that of Se isotopes and TOC/TS (Fig. 3E). These observations suggest that the organic Se fraction exerted the dominant influence on the bulk-rock $\delta^{82/78}Se$ composition, which is consistent with the nutrient-trap hypothesis and a progressive enrichment of heavy Se isotopes in the salt wedge toward the landward portion of the basin. Further phase-specific Se isotope work (cf. Stüeken et al., 2015c) would help to resolve the role of multi-component mixing on bulk rock Se isotopic variability in the geologic record, particularly if future studies individually characterize the organic, sulfide and Se^0 phases.

6.2. Late Devonian: Effect of watermass restriction on Se isotope ratios

The deposition of black shales in the Late Devonian NAS provides another case study of Se burial and isotopic fractionation in basins with variable redox and hydrographic conditions (Algeo et al., 2007). As in the Late Pennsylvanian NAMS, considerable Se isotopic variability is observed between units, with $\delta^{82/78}Se$ values spanning much of the range observed in the geologic record. As in the NAMS dataset, the $\delta^{82/78}Se$ of NAS black shales correlates only weakly with TOC/TS ratios (Fig. 6A), suggesting that variable mixing of organic- and sulfide-bound Se fractions is not the dominant control on bulk-rock $\delta^{82/78}Se$ compositions.

For the NAS dataset, $\delta^{82/78}Se$ shows significant negative covariation with $\delta^{15}N$ (Fig. 6B). One possible explanation for this relationship is that watermasses with near-zero $\delta^{15}N$ values – which reflect systems with scarce nitrate and dominated by nitrogen fixation (Ader et al., 2016; Stüeken et al., 2016) – are also depleted in Se oxyanions, since Se reduction is initiated at redox potentials similar to denitrification (Fig. 1). This scenario may be typical of more restricted settings in which nitrate is not readily replenished from a seawater source. Over time, such basins would tend to deplete their nitrate reservoirs, leading to strong nitrogen fixation as observed in the modern Black Sea (Fulton et al., 2012). A concurrent depletion of Se oxyanions would result in progressive enrichment of heavy isotopes in the residual aqueous Se reservoir (it is important to note that the Se cycle has no equivalent to N_2 fixation, *i.e.,* there is no source of isotopically light Se upon depletion of the Se oxyanion reservoir.) This inference is supported by the positive correlation between Se concentrations and $\delta^{15}N$ values in the NAS black shales (Fig. 6C). Units with near-zero $\delta^{15}N$ values indicative of a limited aqueous nitrate reservoir also tend to have low Se contents (~1 μg/g or less). The only samples with Se concentrations > 10 ppm also have $\delta^{15}N$ close to that of modern seawater nitrate (~+5‰), which is consistent with a close linkage between N and Se cycling. As bottom water redox conditions were more-or-less uniformly anoxic across all of the NAS basins (Algeo et al., 2007), we infer that differences in $\delta^{82/78}Se$ between study units in different basins were due to variable degrees of basinal restriction and seawater renewal times.

Another way to test this hypothesis is to look for evidence of basinal restriction in other geochemical proxies. Basinal restriction commonly results in development of non-marine salinities, and paleosalinity variation in shale facies can be inferred from Sr/Ba ratios (Wei et al., 2018; Wei and Algeo, 2019, this issue). Across the NAS units sampled here, average Sr/Ba ratios range from 0.16 to 0.45 (Fig. 5; Table 4), which is consistent with mostly brackish (0.2–0.5) rather than marine salinity conditions (>0.5, as defined by Wei and Algeo, 2019, this issue). Thus, all of the interior NAS basins show a degree of watermass restriction, promoting mixing of seawater with freshwater runoff from the Laurentian Craton. However, unit-average Sr/Ba does not correlate strongly with $\delta^{82/78}Se$ ($R^2 = 0.07$), perhaps because salinity and seawater renewal times are not strongly coupled in restricted-basinal settings (cf. Algeo and Lyons, 2006). Mo/TOC ratios can also reflect the degree of basinal restriction if bottom-water redox conditions are uniform (Algeo and Lyons, 2006), which is approximately true of NAS black shales (Algeo et al., 2007; note that the bioturbated gray shale horizons of the New Albany Shale were excluded from this analysis because bioturbation implies at least transiently oxic conditions). In contrast to Sr/Ba, unit-average Mo/TOC exhibits a strong negative correlation with $\delta^{82/78}Se$ (Fig. 7), which may indicate a hydrographic control on $\delta^{82/78}Se$ in the NAS. Specifically, more restricted basins in which aqueous Mo is strongly depleted also tend to become more enriched in heavy Se isotopes as their Se reservoir is drawn down. We note that the $\delta^{82/78}Se$ vs. Mo/TOC relationship is based on relatively few data (6 units), but it is supported by the Se-$\delta^{15}N$ relationships discussed above and by Sr/Ba evidence of generally brackish conditions, all of which are consistent with basinal restriction imparting a strong influence on Se isotopic compositions in the Late Devonian NAS.

The implication for controls on $\delta^{82/78}Se$ compositions is that deep-water renewal in less restricted basins can replenish Se oxyanions, providing a larger Se reservoir that is less prone to quantitative reduction. This process can account for lower $\delta^{82/78}Se$ in the Woodford Shale of the relatively open Oklahoma Basin relative to the more-restricted Appalachian and Illinois basin black shales. These data demonstrate the influence of basin hydrography on $\delta^{82/78}Se$ values in reducing marine sediments, as previously inferred based on more limited evidence (Stüeken et al., 2015b). The implication for the use of $\delta^{82/78}Se$ values as a paleo-redox proxy is that strongly restricted basins may not record signals that are representative of Se cycling in the open ocean. The marked enrichment of heavy Se isotopes in anoxic horizons of the New Albany Shale provides no evidence of non-quantitative oxyanion reduction, which could be interpreted as evidence of an anoxic deep ocean. However, the Woodford Shale, which was accumulating at the same time and in closer proximity to the open ocean (and with a shorter renewal time, as inferred from the higher Mo/TOC ratios; Fig. 5; Algeo et al., 2007), recorded

Please cite this article in press as: Kipp M. A., et al. Basinal hydrographic and redox controls on selenium enrichment and isotopic composition in Paleozoic black shales. *Geochim. Cosmochim. Acta* (2020), https://doi.org/10.1016/j.gca.2019.12.016

modern-seawater-like $\delta^{82/78}$Se values, which may be more representative of global Se cycling during the late Devonian. We therefore recommend that, when employing the Se isotope proxy in deep time, complementary datasets such as δ^{15}N, Sr/Ba and Mo/TOC be generated and evaluated across differing formations of similar age and setting. Although each paleoenvironmental proxy faces its own limitations, a combined approach allows the strongest possible inferences about ancient watermass chemistry. This will be particularly important for application of Se isotopes in the Precambrian, where comparatively little is known about the paleogeographic context of black shale basins.

6.3. Comparing controls on Se in Upper Pennsylvanian and Upper Devonian black shales

We close by comparing and contrasting the dominant controls on Se enrichment and isotopic fractionation between shales deposited in the Late Pennsylvanian NAMS and the Late Devonian NAS. The most pronounced difference between these two ancient seaways is that Se concentrations reach far higher levels in the NAMS (particularly on the Midcontinent Shelf) than in any of the Late Devonian NAS basins (Fig. 8). Several factors are likely to have contributed to this difference.

First, as noted in Section 6.2, the Late Devonian NAS basins appear to have been more restricted (as evidenced by lower Sr/Ba ratios; Fig. 8) than the Midcontinent Shelf and Illinois Basin in the Late Pennsylvanian. Due to slower seawater renewal times, the waters overlying the NAS shales became depleted in nitrate (as evidenced by lower δ^{15}N values) and likely also Se oxyanions (as evidenced by lower Se enrichment; Fig. 8). Importantly, these differences do not correspond to variations in TOC or TS content (Fig. 8), suggesting that the capacity for Se enrichment was limited in the NAS basins despite similarly anoxic bottom water conditions and a similar capacity for shuttling trace metals to deep waters. These considerations highlight the importance of basinal hydrography in controlling the degree of Se enrichment in restricted marine basins.

Second, the processes by which Se became enriched in the sediment differed between the Late Pennsylvanian and Late Devonian seaways. As described in Section 6.1, Se enrichment on the Midcontinent Shelf of the NAMS was likely due to a nutrient-trapping mechanism linked to its quasi-estuarine circulation pattern (Algeo et al., 2008a, 2008b; Algeo and Herrmann, 2018). These conditions not only promoted strong Se uptake by the sediment but also led to significantly greater Se enrichment relative to other redox-sensitive trace metals, including Mo, U and V (Fig. 9). This pattern was probably due to Se being shuttled to deep waters mainly via sinking organic matter, which was more efficiently recycled in the water column than the Fe-Mn-oxides that transported trace metals such as Mo to the sediment-water interface. In contrast, the Late Devonian NAS basins, which were not characterized by the same sort of nutrient trap, show Se enrichments that are on par with other redox-sensitive trace metals such as U and V (Fig. 9B, C), and Mo is actually more enriched than Se in some Upper Devonian shales (Fig. 9A). As noted in Section 6.2, depletion of the Se oxyanion reservoirs in the more restricted NAS basins occurred alongside nitrate depletion, but to a lesser degree than Mo depletion. This suggests that Se was being reductively immobilized at relatively high redox potentials, similar to nitrate reduction but above the redox potential at which Mo is efficiently scavenged (cf. Helz et al., 1996), impeding quantitative removal of aqueous Mo to the sediment. Thus, including Se in paleoredox studies can provide additional insights into water column redox thresholds by adding a high-redox-potential species to the arsenal of trace-metal-enrichment proxies (cf. Tribovillard et al., 2006).

An important implication of both datasets is that bulk-rock $\delta^{82/78}$Se values in restricted basins can substantially diverge from open-ocean signatures. For deep-time applications of the $\delta^{82/78}$Se proxy, it is therefore imperative to constrain the degree of open-ocean exchange when interpreting $\delta^{82/78}$Se data in the context of global redox evolution. In the present study, we found that combining $\delta^{82/78}$Se data with proxies for basinal restriction (Sr/Ba, Mo/TOC) and redox

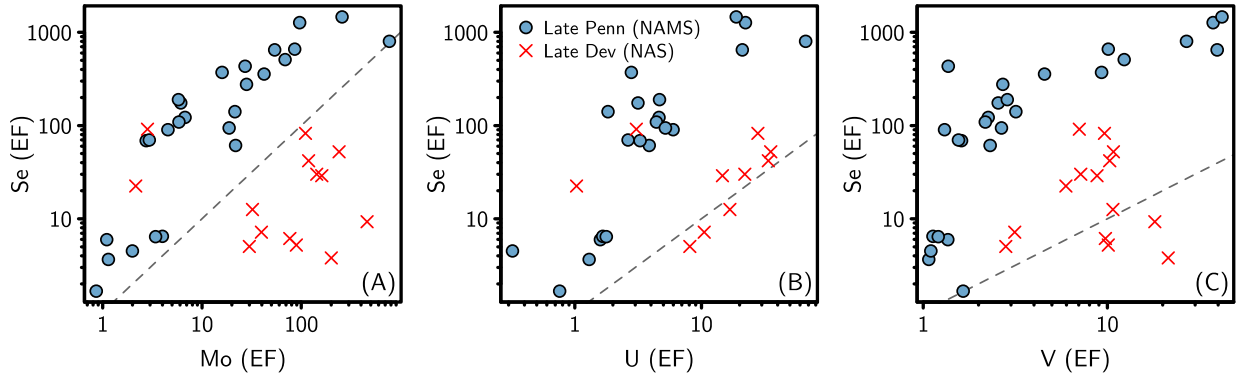

Fig. 9. **Selenium enrichment factors relative to molybdenum (A), uranium (B) and vanadium (C).** The greater enrichment of Se relative to other redox-sensitive trace metals in the NAMS shales suggests that Se was more effectively recycled by the estuarine nutrient trap. In contrast, Se is not preferentially enriched relative to U and V in the NAS black shales, which did not feature a nutrient trap. The higher Mo enrichment relative to Se in the NAS samples may reflect depletion of the aqueous Se reservoir faster than the Mo reservoir at redox potentials higher than that required for Mo scavenging (*i.e.*, euxinic conditions).

Please cite this article in press as: Kipp M. A., et al. Basinal hydrographic and redox controls on selenium enrichment and isotopic composition in Paleozoic black shales. *Geochim. Cosmochim. Acta* (2020), https://doi.org/10.1016/j.gca.2019.12.016

chemistry ($\delta^{15}N$, Fe/Al, DOP) provided a useful context for evaluating the significance of Se isotopic variations. Such an integrated approach will be critical in order to make the most effective use of $\delta^{82/78}Se$ as a proxy for Earth's secular oxygenation history.

7. CONCLUSIONS

We have analyzed Se concentrations and isotope ratios in a range of black shales deposited in epicontinental seas in the late Paleozoic. When viewed within the context provided by other major and trace elemental data, the Se data seem to reflect differences in both local redox conditions and basinal hydrography. On the Midcontinent Shelf of the Late Pennsylvanian NAMS, a quasi-estuarine nutrient trap concentrated Se and other trace metals in saline deep waters that became progressively isotopically enriched through successive recycling of organic-bound Se. In contrast, isotopic variability among basins in the Late Devonian NAS appears to have been controlled by differing hydrographic conditions, where more restricted settings featured Se oxyanion reduction alongside nitrate reduction with limited re-supply from the open marine reservoir. This caused the more restricted basins to display lower Se abundances and stronger isotopic enrichment, in contrast to settings that received greater seawater influx. In both the NAMS and NAS datasets, the additional context provided by TOC, TS, Mo/TOC, Sr/Ba, Fe/Al, DOP, and $\delta^{15}N$ greatly helped in resolving the environmental drivers of variability in Se abundance and isotopic composition, although we also note that the dominant biogeochemical controls on the Se cycle are not captured by any one of those proxies alone. Extending these findings to other paleo-environmental settings, our results suggest that restricted basins are prone to record enrichment of heavy Se isotopes if not regularly replenished with a seawater source of Se oxyanions, which can make these settings unsuitable for assessing global redox conditions. The future utilization of Se isotopes as a paleo-redox proxy will greatly benefit from a concerted effort to make high-precision, phase-specific measurements, as well as from the use of complementary datasets to resolve aspects of basinal redox and hydrography that can provide critical context for Se isotopic interpretations.

Declaration of Competing Interest

The authors declare that they have no known competing financial interests or personal relationships that could have appeared to influence the work reported in this paper.

ACKNOWLEDGMENTS

We thank Scott Kuehner, Fang-Zhen Teng, Bruce Nelson, Yan Hu and Andy Schauer for technical support. This work was supported by an NSF Graduate Research Fellowship to MAK (DGE-1256082) and a NASA Exobiology grant to RB (NNX16AI37G). TJA thanks the state geological surveys of Ohio, Kentucky, Tennessee, New York, Illinois, Kansas, Oklahoma, and North Dakota for providing access to cores sampled for studies of Upper Pennsylvanian and Upper Devonian black shales, and Jeff Over for providing samples from three locales of the Woodford Formation. Three anonymous reviewers are thanked for comments that substantively improved this manuscript.

APPENDIX A. SUPPLEMENTARY MATERIAL

Supplementary data to this article can be found online at https://doi.org/10.1016/j.gca.2019.12.016.

REFERENCES

Ader M., Thomazo C., Sansjofre P., Busigny V., Papineau D., Laffont R., Cartigny P. and Halverson G. P. (2016) Interpretation of the nitrogen isotopic composition of Precambrian sedimentary rocks: Assumptions and perspectives. *Chem. Geol.* **429**, 93–110.

Algeo T. J. and Heckel P. H. (2008) The Late Pennsylvanian midcontinent sea of North America: a review. *Palaeogeogr. Palaeoclimatol. Palaeoecol.* **268**, 205–221.

Algeo T. J. and Herrmann A. D. (2018) An ancient estuarine-circulation nutrient trap: The Late Pennsylvanian Midcontinent Sea of North America. *Geology* **46**, 143–146.

Algeo T. J. and Lyons T. W. (2006) Mo–total organic carbon covariation in modern anoxic marine environments: Implications for analysis of paleoredox and paleohydrographic conditions. *Paleoceanography* **21**.

Algeo T. J. and Maynard J. B. (2004) Trace-element behavior and redox facies in core shales of Upper Pennsylvanian Kansas-type cyclothems. *Chem. Geol.* **206**, 289–318.

Algeo T. J. and Maynard J. B. (2008) Trace-metal covariation as a guide to water-mass conditions in ancient anoxic marine environments. *Geosphere* **4**, 872–887.

Algeo T. J. and Tribovillard N. (2009) Environmental analysis of paleoceanographic systems based on molybdenum–uranium covariation. *Chem. Geol.* **268**, 211–225.

Algeo T. J., Lyons T. W., Blakey R. C. and Over D. J. (2007) Hydrographic conditions of the Devono-Carboniferous North American Seaway inferred from sedimentary Mo–TOC relationships. *Palaeogeogr. Palaeoclimatol. Palaeoecol.* **256**, 204–230.

Algeo T. J., Heckel P. H., Maynard J. B., Blakey R., Rowe H., Pratt B. R. and Holmden C. (2008a) Modern and ancient epeiric seas and the super-estuarine circulation model of marine anoxia. *Dyn. Epeiric Seas Sedimentol. Paleontol. Geochem. Perspect. St Johns Can Geol. Assoc. Can. Spec. Publ.* **48**, 7–38.

Algeo T. J., Rowe H., Hower J. C., Schwark L., Herrmann A. and Heckel P. H. (2008b) Oceanic denitrification during Late Carboniferous glacial-interglacial cycles. *Nat. Geosci.* **1**, 709–714.

Algeo T. J., Morford J. and Cruse A. (2012) New applications of trace metals as proxies in marine paleoenvironments. *Chem. Geol.* **306–307**, 160–164.

Anbar A. D. and Gordon G. W. (2008) Redox renaissance. *Geology* **36**(3), 271–272.

Anderson R. F., Sachs J. P., Fleisher M. Q., Allen K. A., Yu J., Koutavas A. and Jaccard S. L. (2019) Deep-sea oxygen depletion and ocean carbon sequestration during the last ice age. *Global Biogeochem. Cy.* **33**, 301–317.

Arnold G. L., Anbar A. D., Barling J. and Lyons T. W. (2004) Molybdenum isotope evidence for widespread anoxia in mid-proterozoic oceans. *Science* **304**, 87–90.

Audry S., Blanc G., Schäfer J., Chaillou G. and Robert S. (2006) Early diagenesis of trace metals (Cd, Cu Co, Ni, U, Mo, and V) in the freshwater reaches of a macrotidal estuary. *Geochim. Cosmochim. Acta* **70**, 2264–2282.

Balistrieri L. S. and Chao T. T. (1990) Adsorption of selenium by amorphous iron oxyhydroxide and manganese dioxide. *Geochim. Cosmochim. Acta* **54**, 739–751.

Basu A., Schilling K., Brown S. T., Johnson T. M., Christensen J. N., Hartmann M., Reimus P. W., Heikoop J. M., Woldegabriel G. and DePaolo D. J. (2016) Se isotopes as groundwater redox indicators: detecting natural attenuation of Se and in in situ recovery U mine. *Environ. Sci. Technol.* **50**, 10833–10842.

Broecker W. S. and Peng T.-H. (1982) *Tracers in the Sea*. Lamont-Doherty Geological Observatory, Columbia University.

Brumsack H.-J. (2006) The trace metal content of recent organic carbon-rich sediments: implications for Cretaceous black shale formation. *Palaeogeogr. Palaeoclimatol. Palaeoecol.* **232**, 344–361.

Calvert S. E., Bustin R. M. and Ingall E. D. (1996) Influence of water column anoxia and sediment supply on the burial and preservation of organic carbon in marine shales. *Geochim. Cosmochim. Acta* **60**, 1577–1593.

Carignan J. and Wen H. (2007) Scaling NIST SRM 3149 for Se isotope analysis and isotopic variations of natural samples. *Chem. Geol.* **242**, 347–350.

Chang Y., Zhang J., Qu J.-Q. and Xue Y. (2017) Precise selenium isotope measurement in seawater by carbon-containing hydride generation-Desolvation-MC-ICP-MS after thiol resin preconcentration. *Chem. Geol.* **471**, 65–73.

Chau Y. K. and Riley J. P. (1965) The determination of selenium in sea water, silicates and marine organisms. *Anal. Chim. Acta* **33**, 36–49.

Chen X., Ling H.-F., Vance D., Shields-Zhou G. A., Zhu M., Poulton S. W., Och L. M., Jiang S.-Y., Li D. and Cremonese L. (2015) Rise to modern levels of ocean oxygenation coincided with the Cambrian radiation of animals. *Nat. Commun.* **6**, 7142.

Clark S. K. and Johnson T. M. (2010) Selenium stable isotope investigation into selenium biogeochemical cycling in a lacustrine environment: Sweitzer Lake, Colorado. *J. Environ. Qual.* **39**, 2200–2210.

Clarkson Matthew O., Stirling Claudine H., Jenkyns Hugh C., Dickson Alexander J., Porcelli Do, Moy Christopher M., Pogge von Strandmann Philip A. E., Cooke Ilsa R. and Lenton Timothy M. (2018) Uranium isotope evidence for two episodes of deoxygenation during Oceanic Anoxic Event 2. *Proc. Natl. Acad. Sci. U.S.A.* **115**(12), 2918–2923. https://doi.org/10.1073/pnas.1715278115.

Conde J. E. and Alaejos M. S. (1997) Selenium concentrations in natural and environmental waters. *Chem. Rev.* **97**, 1979–2004.

Coplen T. B., Brand W. A., Gehre M., Gröning M., Meijer H. A., Toman B. and Verkouteren R. M. (2006) New guidelines for $\delta^{13}C$ measurements. *Anal. Chem.* **78**, 2439–2441.

Cruse A. M. and Lyons T. W. (2004) Trace metal records of regional paleoenvironmental variability in Pennsylvanian (Upper Carboniferous) black shales. *Chem. Geol.* **206**, 319–345.

Cutter G. A. and Bruland K. W. (1984) The marine biogeochemistry of selenium: A re-evaluation. *Limnol. Oceanogr.* **29**, 1179–1192.

Dahl T. W., Hammarlund E. U., Anbar A. D., Bond D. P. G., Gill B. C., Gordon G. W., Knoll A. H., Nielsen A. T., Schovsbo N. H. and Canfield D. E. (2010) Devonian rise in atmospheric oxygen correlated to the radiations of terrestrial plants and large predatory fish. *Proc. Natl. Acad. Sci. (U.S.A.)* **107**, 17911–17915.

Ellis A. S., Johnson T. M., Herbel M. J. and Bullen T. D. (2003) Stable isotope fractionation of selenium by natural microbial consortia. *Chem. Geol.* **195**, 119–129.

Fan H., Wen H., Hu R. and Zhao H. (2011) Selenium speciation in Lower Cambrian Se-enriched strata in South China and its geological implications. *Geochim. Cosmochim. Acta* **75**, 7725–7740.

Floor G. H. and Román-Ross G. (2012) Selenium in volcanic environments: A review. *Appl. Geochem.* **27**, 517–531.

Fry B., Silva S. R., Kendall C. and Anderson R. K. (2002) Oxygen isotope corrections for online $\delta^{34}S$ analysis. *Rapid Commun. Mass Spectrom.* **16**, 854–858.

Fulton J. M., Arthur M. A. and Freeman K. H. (2012) Black Sea nitrogen cycling and the preservation of phytoplankton $\delta^{15}N$ signals during the Holocene. *Glob. Biogeochem. Cycles*, 26.

Gordon G. W., Lyons T. W., Arnold G. L., Roe J., Sageman B. B. and Anbar A. D. (2009) When do black shales tell molybdenum isotope tales? *Geology* **37**, 535–538.

Hartwell W. J. (1998) Geochemical and petrographic analysis of the Upper Devonian-Lower Mississippian Bakken black shales from the Williston Basin, North Dakota. Master's Thesis, University of Cincinnati, Cincinnati, Ohio.

Heckel P. H. (1977) Origin of phosphatic black shale facies in Pennsylvanian cyclothems of mid-continent North America. *AAPG Bull.* **61**, 1045–1068.

Heckel P. H. (1994) Evaluation of evidence for glacio-eustatic control over marine Pennsylvanian cyclothems in North America and consideration of possible tectonic effects. In *Tectonic and Eustatic Controls on Sedimentary Cycles* (eds. J. M. Dennison and F. R. Ettensohn). SEPM, Concepts in Sedimentology and Paleontology, pp. 65–87.

Helz G. R., Miller C. V., Charnock J. M., Mosselmans J. L. W., Pattrick R. A. D., Garner C. D. and Vaughan D. J. (1996) Mechanisms of molybdenum removal from the sea and its concentration in black shales: EXAFS evidences. *Geochim. Cosmochim. Acta* **60**, 3631–3642.

Herrmann A. D., Barrick J. E. and Algeo T. J. (2015) The relationship of conodont biofacies to spatially variable watermass properties in the Late Pennsylvanian Midcontinent Sea. *Paleoceanography* **30**(3), 269–283.

Herrmann A. D., Barrick J. E., Algeo T. J. and Peng Y. B. (2019) Conodont biofacies and watermass structure of the Middle Pennsylvanian North American Midcontinent Sea. *Palaeoclimatol. Palaeoecol. Palaeogeogr.*. https://doi.org/10.1016/j.palaeo.2019.109235.

Ingall E. D., Bustin R. M. and Van Cappellen P. (1993) Influence of water column anoxia on the burial and preservation of carbon and phosphorus in marine shales. *Geochim. Cosmochim. Acta* **57**, 303–316.

Jaminski J. (1997) Geochemical and petrographic patterns of cyclicity in the Devonian-Mississippian black shales of the Central Appalachian Basin. Ph. D. dissertation, University of Cincinnati, Cincinnati, Ohio.

Jaminski J., Algeo T. J., Maynard J. B. and Hower J. C. (1998) Climatic origin of dm-scale compositional cyclicity in the Cleveland Member of the Ohio Shale (Upper Devonian), Central Appalachian Basin, USA. In *Shales and Mudstones* (eds. J. Schieber, W. Zimmerle and P. S. Sethi). v. 1: Stuttgart, Schweizerbart'sche, pp. 217–242.

Jimenez M. Y., Ivany L. C., Judd E. J. and Henkes G. (2019) Low and seasonally variable salinity in the Pennsylvanian equatorial Appalachian Basin. *Earth Planet. Sci. Lett.* **519**, 182–191.

Joachimski M. M. and Lambert L. L. (2015) Salinity contrast in the US Midcontinent Sea during Pennsylvanian glacio-eustatic highstands: Evidence from conodont apatite $\delta^{18}O$. *Palaeogeogr. Palaeoclimatol. Palaeoecol.* **433**, 71–80.

Johnson T. M. and Bullen T. D. (2003) Selenium isotope fractionation during reduction by Fe(II)-Fe(III) hydroxide-sulfate (green rust). *Geochim. Cosmochim. Acta* **67**, 413–419.

Please cite this article in press as: Kipp M. A., et al. Basinal hydrographic and redox controls on selenium enrichment and isotopic composition in Paleozoic black shales. *Geochim. Cosmochim. Acta* (2020), https://doi.org/10.1016/j.gca.2019.12.016

Johnson T. M. and Bullen T. D. (2004) Mass-dependent fractionation of selenium and chromium isotopes in low-temperature environments. *Rev. Mineral. Geochem.* **55**, 289–317.

Johnson T. M., Herbel M. J., Bullen T. D. and Zawislanski P. T. (1999) Selenium isotope ratios as indicators of selenium sources and oxyanion reduction. *Geochim. Cosmochim. Acta* **63**, 2775–2783.

Kendall B., Dahl T. W. and Anbar A. D. (2017) The stable isotope geochemistry of molybdenum. *Rev. Mineral. Geochem.* **82**, 683–732.

Kendall B., Gordon G. W., Poulton S. W. and Anbar A. D. (2011) Molybdenum isotope constraints on the extent of late Paleoproterozoic ocean euxinia. *Earth Planet. Sci. Lett.* **307**, 450–460.

Kendall B., Komiya T., Lyons T. W., Bates S. M., Gordon G. W., Romaniello S. J., Jiang G., Creaser R. A., Xiao S., McFadden K., Sawaki Y., Tahata M., Shu D., Han J., Li Y., Chu X. and Anbar A. D. (2015) Uranium and molybdenum isotope evidence for an episode of widespread ocean oxygenation during the late Ediacaran Period. *Geochim. Cosmochim. Acta* **156**, 173–193.

Kipp M. A., Stüeken E. E., Bekker A. and Buick R. (2017) Selenium isotopes record extensive marine suboxia during the Great Oxidation Event. *Proc. Natl. Acad. Sci. (U.S.A.)* **114**, 875–880.

Kipp M. A., Stüeken E. E., Yun M., Bekker A. and Buick R. (2018) Pervasive aerobic nitrogen cycling in the surface ocean across the Paleoproterozoic Era. *Earth Planet. Sci. Lett.* **500**, 117–126.

Koehler M. C., Buick R., Kipp M. A., Stüeken E. E. and Zaloumis J. (2018) Transient surface ocean oxygenation recorded in the ~2.66 Ga Jeerinah Formation, Australia. *Proc. Natl. Acad. Sci. (U.S.A.)* **115**, 7711–7716.

Kulp T. R. and Pratt L. M. (2004) Speciation and weathering of selenium in Upper Cretaceous chalk and shale from South Dakota and Wyoming, USA. *Geochim. Cosmochim. Acta* **68**, 3687–3701.

Kurzawa T., König S., Labidi J., Yierpan A. and Schoenberg R. (2017) A method for Se isotope analysis of low ng-level geological samples via double spike and hydride generation MC-ICP-MS. *Chem. Geol.* **466**, 219–228.

Large R. R., Halpin J. A., Danyushevsky L. V., Maslennikov V. V., Bull S. W., Long J. A., Gregory D. D., Lounejeva E., Lyons T. W. and Sack P. J. (2014) Trace element content of sedimentary pyrite as a new proxy for deep-time ocean–atmosphere evolution. *Earth Planet. Sci. Lett.* **389**, 209–220.

Lash G. G. (2017) A multiproxy analysis of the Frasnian-Famennian transition in western New York State, U.S.A. *Palaeogeogr. Palaeoclimatol. Palaeoecol.* **473**, 108–122.

Lau K. V., Macdonald F. A., Maher K. and Payne J. L. (2017) Uranium isotope evidence for temporary ocean oxygenation in the aftermath of the Sturtian Snowball Earth. *Earth Planet. Sci. Lett.* **458**, 282–292.

Lau K. V., Maher K., Altiner D., Kelley B. M., Kump L. R., Lehrmann D. J., Silva-Tamayo J. C., Weaver K. L., Yu M. and Payne J. L. (2016) Marine anoxia and delayed Earth system recovery after the end-Permian extinction. *Proc. Natl. Acad. Sci. (U.S.A.)* **113**, 2360–2365.

Lineback J. A. (1970) *Stratigraphy of the New Albany Shale in Indiana*. State of Indiana, Department of Natural Resources.

Little S. H., Vance D., Lyons T. W. and McManus J. (2015) Controls on trace metal authigenic enrichment in reducing sediments: Insights from modern oxygen-deficient settings. *Am. J. Sci.* **315**, 77–119.

Lu W., Ridgwell A., Thomas E., Hardisty D. S., Luo G., Algeo T. J., Saltzman M. R., Gill B. C., Shen Y., Ling H.-F., Edwards C. T., Whalen M. T., Zhou X., Gutchess K. M., Jin L., Rickaby R. E. M., Jenkyns H. C., Lyons T. W., Lenton T. M., Kump L. R. and Lu Z. (2018) Late inception of a resiliently oxygenated upper ocean. *Science* **361**, 174–177.

Lu Z., Jenkyns H. C. and Rickaby R. E. M. (2010) Iodine to calcium ratios in marine carbonate as a paleo-redox proxy during oceanic anoxic events. *Geology* **38**, 1107–1110.

Lyons T. W., Reinhard C. T. and Planavsky N. J. (2014) The rise of oxygen in Earth's early ocean and atmosphere. *Nature* **506**, 307–315.

Martens D. A. and Suarez D. L. (1997) Selenium speciation of marine shales, alluvial soils, and evaporation basin soils of California. *J. Environ. Qual.* **26**, 424–432.

Measures C. I. and Burton J. D. (1980) The vertical distribution and oxidation states of dissolved selenium in the northeast Atlantic Ocean and their relationship to biological processes. *Earth Planet. Sci. Lett.* **46**, 385–396.

Measures C. I., McDuff R. E. and Edmond J. M. (1980) Selenium redox chemistry at GEOSECS I re-occupation. *Earth Planet. Sci. Lett.* **49**, 102–108.

Mitchell K., Mansoor S. Z., Mason P. R. D., Johnson T. M. and Van Cappellen P. (2016) Geological evolution of the marine selenium cycle: Insights from the bulk shale $\delta^{82/76}$Se record and isotope mass balance modeling. *Earth Planet. Sci. Lett.* **441**, 178–187.

Mitchell K., Mason P. R., Van Cappellen P., Johnson T. M., Gill B. C., Owens J. D., Diaz J., Ingall E. D., Reichart G.-J. and Lyons T. W. (2012) Selenium as paleo-oceanographic proxy: A first assessment. *Geochim. Cosmochim. Acta* **89**, 302–317.

Morford J. L. and Emerson S. (1999) The geochemistry of redox sensitive trace metals in sediments. *Geochim. Cosmochim. Acta* **63**, 1735–1750.

Mosher B. W. and Duce R. A. (1987) A global atmospheric selenium budget. *J. Geophys. Res.* **92**, 13289–13298.

Oremland R. S., Hollibaugh J. T., Maest A. S., Presser T. S., Miller L. G. and Culbertson C. W. (1989) Selenate reduction to elemental selenium by anaerobic bacteria in sediments and culture: biogeochemical significance of a novel, sulfate-independent respiration. *Appl. Env. Microbiol.* **55**, 2333–2343.

Over D. J. (1992) Conodonts and the Devonian-Carboniferous boundary in the upper Woodford Shale, Arbuckle Mountains, south-central Oklahoma. *J. Paleontol.* **66**, 293–311.

Over D. J. (2002) The Frasnian/Famennian boundary in central and eastern United States. *Palaeogeogr. Palaeoclimatol. Palaeoecol.* **181**, 153–169.

Over D. J., Hauf E., Wallace J., Chiarello J., Over J. S., Gilleaudeau G. J., Song Y. and Algeo T. J. (2019) Conodont biostratigraphy and magnetic susceptibility of Upper Devonian Chattanooga Shale, eastern United States: Evidence for episodic deposition and disconformities. *Palaeogeogr. Palaeoclimatol. Palaeoecol.* **524**, 137–149.

Partin C. A., Bekker A., Planavsky N. J., Scott C. T., Gill B. C., Li C., Podkovyrov V., Maslov A., Konhauser K. O., Lalonde S. V., Love G. D., Poulton S. W. and Lyons T. W. (2013) Large-scale fluctuations in Precambrian atmospheric and oceanic oxygen levels from the record of U in shales. *Earth Planet. Sci. Lett.* **369**, 284–293.

Pogge von Strandmann P. A. E., Coath C. D., Catling D. C., Poulton S. W. and Elliott T. (2014) Analysis of mass dependent and mass independent selenium isotope variability in black shales. *J. Anal. At. Spectrom.* **29**, 1648–1659.

Pogge von Strandmann P. A. E., Stüeken E. E., Elliott T., Poulton S. W., Dehler C. M., Canfield D. E. and Catling D. C. (2015) Selenium isotope evidence for progressive oxidation of the Neoproterozoic biosphere. *Nat. Commun.*, 6.

Please cite this article in press as: Kipp M. A., et al. Basinal hydrographic and redox controls on selenium enrichment and isotopic composition in Paleozoic black shales. *Geochim. Cosmochim. Acta* (2020), https://doi.org/10.1016/j.gca.2019.12.016

Qie W. K., Algeo T. J., Luo G. M. and Herrmann A. D. (2019) Global events of the Early Devonian to Middle Permian: A review. *Palaeoclimatol. Palaeoecol. Palaeogeogr.*. https://doi.org/10.1016/j.palaeo.2019.109259.

Roark A., Flake R., Grossman E. L., Olszewski T., Lebold J., Thomas D., Marcantonio F., Miller B., Raymond A. and Yancey T. (2017) Brachiopod geochemical records from across the Carboniferous seas of North America: Evidence for salinity gradients, stratification, and circulation patterns. *Palaeogeogr. Palaeoclimatol. Palaeoecol.* **485**, 136–153.

Rouxel O., Ludden J., Carignan J., Marin L. and Fouqet Y. (2002) Natural variations of Se isotopic composition determined by hydride generation multiple collector inductively coupled plasma mass spectrometry. *Geochim. Cosmochim. Acta* **66**, 3191–3199.

Rouxel O., Fouquet Y. and Ludden J. N. (2004) Subsurface processes at the Lucky Strike hydrothermal field, Mid-Atlantic Ridge: evidence from sulfur, selenium, and iron isotopes. *Geochim. Cosmochim. Acta* **68**, 2295–2311.

Rovira M., Giménez J., Martínez M., Martínez-Lladó X., de Pablo J., Marti V. and Duro L. (2008) Sorption of selenium (IV) and selenium (VI) onto natural iron oxides: goethite and hematite. *J. Hazard. Mater.* **150**, 279–284.

Rue E. L., Smith G. J., Cutter G. A. and Bruland K. W. (1997) The response of trace element redox couples to suboxic conditions in the water column. *Deep Sea Res. Part Oceanogr. Res. Pap.* **44**, 113–134.

Sageman B. B., Murphy A. E., Werne J. P., Ver Straeten C. A., Hollander D. J. and Lyons T. W. (2003) A tale of shales: the relative roles of production, decomposition, and dilution in the accumulation of organic-rich strata, Middle-Upper Devonian, Appalachian basin. *Chem. Geol.* **195**, 229–273.

Schilling K., Johnson T. M. and Mason P. R. (2014) A sequential extraction technique for mass-balanced stable selenium isotope analysis of soil samples. *Chem. Geol.* **381**, 125–130.

Schilling K., Johnson T. M. and Wilcke W. (2011) Selenium partitioning and stable isotope ratios in urban topsoils. *Soil Sci. Soc. Am. J.* **75**, 1354–1364.

Scott C., Lyons T. W., Bekker A., Shen Y., Poulton S. W., Chu X. and Anbar A. D. (2008) Tracing the stepwise oxygenation of the Proterozoic ocean. *Nature* **452**, 456–U5.

Shiller A. M. (1996) The effect of recycling traps and upwelling on estuarine chemical flux estimates. *Geochim. Cosmochim. Acta* **60**, 3177–3185.

Shore A. J. T. (2011) *Selenium geochemistry and isotopic composition of sediments from the Cariaco Basin and the Bermuda Rise: a comparison between a restricted basin and the open ocean over the last 500 ka. Ph.D. dissertation*. University of Leicester, Leicester, UK.

Siebert C., Nagler T. F., von Blanckenburg F. and Kramers J. D. (2003) Molybdenum isotope records as a potential new proxy for paleoceanography. *Earth Planet. Sci. Lett.* **211**, 159–171.

Sperling E. A., Frieder C. A., Raman A. V., Girguis P. R., Levin L. A. and Knoll A. H. (2013) Oxygen, ecology, and the Cambrian radiation of animals. *Proc. Natl. Acad. Sci. (U. S. A.)* **110**, 13446–13451.

Stüeken E. E. (2017) Selenium isotopes as a biogeochemical proxy in deep time. *Rev. Mineral. Geochem.* **82**, 657–682.

Stüeken E. E., Buick R. and Anbar A. D. (2015a) Selenium isotopes support free O_2 in the latest Archean. *Geology* **43**, 259–262.

Stüeken E. E., Buick R., Bekker A., Catling D., Foriel J., Guy B. M., Kah L. C., Machel H. G., Montañez I. P. and Poulton S. W. (2015b) The evolution of the global selenium cycle: Secular trends in Se isotopes and abundances. *Geochim. Cosmochim. Acta* **162**, 109–125.

Stüeken E. E., Catling D. C. and Buick R. (2012) Contributions to late Archaean sulphur cycling by life on land. *Nat. Geosci.* **5**, 722–725.

Stüeken E. E., Foriel J., Buick R. and Schoepfer S. D. (2015c) Selenium isotope ratios, redox changes and biological productivity across the end-Permian mass extinction. *Chem. Geol.* **410**, 28–39.

Stüeken E. E., Foriel J., Nelson B. K., Buick R. and Catling D. C. (2013) Selenium isotope analysis of organic-rich shales: advances in sample preparation and isobaric interference correction. *J. Anal. At. Spectrom.* **28**, 1734–1749.

Stüeken E. E., Kipp M. A., Koehler M. C. and Buick R. (2016) The evolution of Earth's biogeochemical nitrogen cycle. *Earth-Sci. Rev.* **160**, 220–239.

Teng F.-Z., Watkins J. M., Dauphas N. and Swainson I. (2017) Non-traditional stable isotopes. *Rev. Mineral. Geochem.* **82**, 885p.

Tesdal J.-E., Galbraith E. D. and Kienast M. (2013) Nitrogen isotopes in bulk marine sediment: linking seafloor observations with subseafloor records. *Biogeosciences* **10**, 101–118.

Tissot F. L. and Dauphas N. (2015) Uranium isotopic compositions of the crust and ocean: Age corrections, U budget and global extent of modern anoxia. *Geochim. Cosmochim. Acta* **167**, 113–143.

Tostevin R., Clarkson M. O., Gangl S., Shields G. A., Wood R. A., Bowyer F., Penny A. M. and Stirling C. H. (2019) Uranium isotope evidence for an expansion of anoxia in terminal Ediacaran oceans. *Earth Planet. Sci. Lett.* **506**, 104–112.

Tribovillard N., Algeo T. J., Lyons T. and Riboulleau A. (2006) Trace metals as paleoredox and paleoproductivity proxies: an update. *Chem. Geol.* **232**, 12–32.

Turner A. C. E., Algeo T. J., Peng Y. and Herrmann A. D. (2019) Circulation patterns in the Late Pennsylvanian North American Midcontinent Sea inferred from spatial gradients in sediment chemsitry and mineralogy. *Palaeoclimatol. Palaeoecol. Palaeogeogr.*. https://doi.org/10.1016/j.palaeo.2018.12.008.

Velinsky D. J. and Cutter G. A. (1990) Determination of elemental selenium and pyrite-selenium in sediments. *Anal. Chim. Acta* **235**, 419–425.

Ver Straeten C. A., Brett C. E. and Sageman B. B. (2011) Mudrock sequence stratigraphy: a multi-proxy (sedimentological, paleobiological and geochemical) approach, Devonian Appalachian Basin. *Palaeogeogr. Palaeoclimatol. Palaeoecol.* **304**, 54–73.

Wei W. and Algeo T. J. (2019) Elemental proxies for paleosalinity analysis of ancient shales and mudrocks. *Cosmochim. Acta Geochim.*. https://doi.org/10.1016/j.gca.2019.06.034.

Wei W., Algeo T. J., Lu Y., Lu Y., Liu H., Zhang S., Peng L., Zhang J. and Chen L. (2018) Identifying marine incursions into the Paleogene Bohai Bay Basin lake system in northeastern China. *Int. J. Coal Geol.* **200**, 1–17.

Wen H. J., Carignan J., Hu R. Z., Fan H. F., Bin C. and Yang G. S. (2007) Large selenium isotope variations and its implication in the Yutangba Se deposit, Hubei Province, China. *Chin. Sci. Bull.* **52**, 2443–2447.

Werne J. P., Sageman B. B., Lyons T. W. and Hollander D. J. (2002) An integrated assessment of a "type euxinic" deposit: evidence for multiple controls on black shale deposition in the Middle Devonian Oatka Creek Formation. *Am. J. Sci.* **302**, 110–143.

Wignall P. B. and Twitchett R. J. (1996) Oceanic anoxia and the end permian mass extinction. *Science* **272**, 1155–1158.

Please cite this article in press as: Kipp M. A., et al. Basinal hydrographic and redox controls on selenium enrichment and isotopic composition in Paleozoic black shales. *Geochim. Cosmochim. Acta* (2020), https://doi.org/10.1016/j.gca.2019.12.016

Yierpan A., Konig S., Labidi J., Kurzawa T., Babechuk M. G. and Schoenberg R. (2018) Chemical sample processing for combined selenium isotope and selenium-tellurium elemental investigation of the earth's igneous reservoirs. *Geochem. Geophy. Geosy.* **19**, 516–533.

Zhang F., Algeo T. J., Romaniello S. J., Cui Y., Zhao L., Chen Z.-Q. and Anbar A. D. (2018) Congruent Permian-Triassic $\delta^{238}U$ records at Panthalassic and Tethyan sites: Confirmation of global-oceanic anoxia and validation of the U-isotope paleo-redox proxy. *Geology* **46**, 327–330.

Zhu J.-M., Johnson T. M., Clark S. K., Zhu X.-K. and Wang X.-L. (2014) Selenium redox cycling during weathering of Se-rich shales: A selenium isotope study. *Geochim. Cosmochim. Acta* **126**, 228–249.

Associate editor: Karen Johannesson